Advanced Control of Permanent Magnet Synchronous Generators for Variable Speed Wind Energy Conversion Systems

by Jacob Hostettler, Bachelor of Science

A Thesis Submitted in Partial
Fulfillment of the Requirements
for the Degree of
Master of Science
in the Field of Electrical Engineering

Advisory Committee:

Xin Wang, Chair

Andy Lozowski

Ying Shang

Graduate School
Southern Illinois University Edwardsville
May, 2015

ABSTRACT

ADVANCED CONTROL OF PERMANENT MAGNET SYNCHRONOUS GENERATORS FOR VARIABLE SPEED WIND ENERGY CONVERSION SYSTEMS

by

JACOB HOSTETTLER

Chairperson: Professor Xin Wang

Various environmental and economic factors have lead to increased global investment in alternative energy technologies such as solar and wind power. Although methodologies for synchronous generator control are well researched, wind turbines present control systems challenges not presented by traditional generation. The varying nature of wind makes achieving synchronism with the power grid a greater challenge. Departing from early use of induction machines, permanent magnet synchronous generators have become the focus of power systems and control systems research into wind energy systems. Their self excited nature, along with their high power density make them ideal. The problem of grid synchronism is alleviated through the use of high performance power electronic AC-AC converters. In order to achieve the highest level of efficiency, advanced control systems techniques become necessary. This work presents the application of two control systems techniques: sliding mode control, and the use of linear matrix inequalities with H_∞ and finite-time boundedness performance criteria. These methods are applied to the dynamical model of a permanent magnet synchronous generator coupled with aerodynamic properties of a variable speed wind energy conversion system. Simulations on the dynamical models are carried out to demonstrate the effectiveness of the proposed control systems methodologies.

ACKNOWLEDGEMENTS

Foremost, I would like to extend my gratitude to Dr. Wang for offering me the opportunity to conduct research with him, and for all of the guidance and instruction he has given me over the past few years. I would like make note of the generous support and instruction given by my graduate committee over the course of my graduate studies. Also, thank you to the excellent faculty at Southern Illinois University Edwardsville, most notably the Electrical and Computer Engineering Department. I would like to extend particular acknowledgment to my good friend research partner Mohammed Jamail Alden Kais to whom I owe much. Lastly, I thank Rebecca Bright and the rest of my family for all of their support and patience throughout my time as a student.

TABLE OF CONTENTS

LIST OF FIGURES

LIST OF TABLES

CHAPTER 1

INTRODUCTION

1.1 Importance

The paradigm shift away from the use of fossil fuels as the primary means of electrical power generation creates necessity for a multitude of new technologies, approaches, and organizational structures within the field. One such prospective technology, Wind energy conversion systems (WECS), seeks to aid in the transition from the collective global reliance on fossil fuels. The necessity for this change stems from a plethora of issues. However, climate change, namely the damages enacted through persistent use of carbon rich fuel sources, prevails as one of the leading arguments in support of this trend. In "Renewable energy: A Response to Climate Change," R.E.H. Sims brings together findings from the International Energy Agency and the United Nations Intergovernmental Panel on Climate Change. Sims argues that the availability of cheap fossil fuels hinders the growth of renewable energy sources, but stresses the necessity of a transition in order to avoid compounding the amount of damage inflicted by the use of fossil fuels for power generation [1]. Another leading argument in favor of reducing a nation's dependence on fossil fuels lies in the desire to achieve energy independence. This concept is addressed in David L. Greene's work "Measuring Energy Security: Can the United States Achieve Oil Independence?" Greene, addresses the economic and security issues associated with reliance on another nation for supply of a desirable commodity [2]. Within the article in *Nature*, "Energy: A Reality Check On the Shale Revolution," J. David Hughes comments on recent resource extraction methods such as hydraulic fracturing. These methods have gained collective attention as a means by which to achieve energy independence, but receive substantial criticism due to the possibility of undesirable environmental repercussions [3]. Increased research into, and implementation of renewable technologies such as wind, could

arguably help expedite or alleviate this dependence. This sentiment is evident in part by the congressional report from Fred Sissine on the "Energy Independence and Security Act of 2007" by the United States of America. The act seeks to address a multitude of issues regarding energy independence. [4].

1.2 Wind Energy Development

The oil problems of the 1970s initiated new research in wind energy, which according to *Optimal Control of Wind Energy Systems: Towards a Global Approach* by I. Munteanu et al., helped propel this former experimental novelty into the increasingly significant role it plays today. The heterogeneous nature of WECS technology gives rise to two main control classifications: power- and speed-control. Power control involves the manipulation of the aerodynamic properties of a wind turbine. Some form of power control, implemented by all WECS in the form of either stall-control or pitch control and active-stall control, sees implementation in all wind turbines. Stall-control reduces aerodynamic efficiency without changing the geometry of the WECS blades, using the stall effect during high winds. As the simplest form of power control, it suffers from disadvantages such as high mechanical stresses. Pitch- and active-stall control modifies the blade geometry through pitch adjustment, while adding complexity, this method offers improved power control. Speed control offers two types of WECS: fixed-speed and variable-speed. Fixed-speed WECS, much as the name implies, operate at a single speed, regardless of wind speed, through direct coupling to the power grid. Variable-speed WECS or VS-WECS see the largest scale implementation, and consequently are the focus of this work. The lack of direct grid coupling results in distinct control flexibility, but requires the use of costly power electronics in order to link the generators to the grid [5]. Therefore the control challenge then becomes achieving the highest level of efficiency from the available wind resource, also known as maximum power point tracking (MPPT). This importance is evident in the continual and recent publication of works such as Maximum Power

Point Tracking Strategy and Direct Torque Control of Permanent Magnet Synchronous Generator Wind Farm by Youssef Errami, et al, [6].

1.3 Permanent Magnet Synchronous Generators

Given various advantages over other generator types, this work focuses on the use of permanent magnet synchronous generators (PMSGs). Although, doubly fed induction generators have seen wide implementation, PMSGs are becoming the more popular form of generation in wind energy. PMSGs. R. Scott Semken, et al. point to the expansion in generation capabilities of wind turbines from the three megawatt range to over six megawatts as a major reason for this shift. The newest of these large designs, often intended for offshore purposes, employ PMSGs. Due to an improved level of reliability, longer life expectancy, improved performance, and lower weight PMSGs exist as a desirable candidate to meet the needs as indicated by their implementation in WECS by companies such as Vestas, GE WIND, and Siemens to name a few [7]. PMSGs also exhibit the distinct advantage of self-excitation [5]. Lack of DC brushes, and the associated maintenance costs, coupled with high efficiency at low speeds and high power to size ratio illuminate the reasons behind the increased employment of PMSGs in in VS-WECS [5], [6]. A popular method of control for electric machines and drives, known as field oriented control (FOC). According to A. Farhan, A. Saleh, and A. Shaltout in High Performance Reluctance Synchronous, FOC offers notable control advantages in electric machine control. FOC involves the transition from the stationary stator reference frame to the stationary rotor reference, reducing the system model from the three equations of the (a, b, c) stationary stator coordinate frame model, to the two equation direct- and quadrature-axis model [8]

1.4 Contribution

This work seeks to incrementally expand on existing research in the field of wind energy by applying existing advanced and non-linear control design techniques for maximum

power point tracking through field oriented control (FOC) of wind energy conversion systems employing permanent magnet synchronous generators (PMSGs). The stationary rotor reference frame PMSG model is derived through the application of Clarkes and Parks transformation methods. First sliding mode control (SMC) techniques are applied towards MPPT of the system. A detailed block model of the system and controller is developed in MATLAB and Simulink. Detailed simulations using a varying wind input are carried out, and the results of the simulations are presented and commented upon. Next, continuous and discrete time control using linear matrix inequalities with robust H_∞ and finite-time boundedness performance criteria are applied to the system. MATLAB solutions of the inequalities provide data on the disturbance responses characteristics of the VS-WECS system. The results of detailed simulations given disturbances applied to the system are presented, and the results are commented upon. Lastly, conclusions drawn upon the results of the simulations presented are presented for consideration.

CHAPTER 2

WIND ENERGY CONVERSION SYSTEM MODELING

As previously stated, the system of interest is a fixed-pitch, variable-speed wind energy conversion system employing a permanent magnet synchronous generator. This WECS construction is given by Fig. 2.1 [5]. The mathematical modeling of the aerodynamics, high speed shaft, and the generator used throughout this wrk have been adapted from the text in [5] and *Wind Energy Control Systems Engineering Design* by Mario Garcia-Sanz and Constantine H. Houpis.

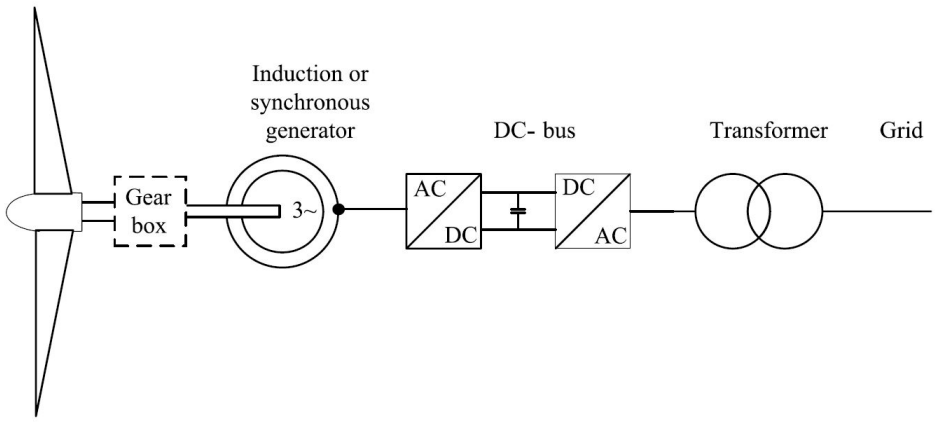

Figure 2.1: WECS Model

2.1 Aerodynamics

The primary input to a WECS is the wind. This wind acts against the blades of the wind turbine, and creates mechanical torque

$$\tau_m = \frac{\rho \pi R_t^2 C_p(\lambda, \beta) v^3}{2\omega_l}, \tag{2.1}$$

where ρ is the air density, R_t is the radius of the rotor, v is the wind speed, and ω_l is the rotational speed of the low speed shaft. The factor $C_p(\lambda, \beta)$ is known as the power

coefficient. It is a function of the tip speed ratio $\lambda = \frac{\omega_l R_t}{v}$, and the blade pitch β. This factor represents the efficiency of mechanical power extracted from an available wind resource, and is found as follows:

$$C_p(\lambda, \beta) = c_1\Big(\frac{c_2}{\lambda_i} - c_3\beta - c_4\Big)e^{-c_5/\lambda_i} \tag{2.2}$$
$$\lambda_i = \Big(\frac{1}{\lambda + c_6\beta} - \frac{c_7}{\beta^3 + 1}\Big)^{-1},$$

where c_1, c_2, c_3, c_4, c_5, and c_6 are constants that depend on the system [5, 9].

Even under ideal assumptions about the performance and construction of a wind turbine a limit exists on the value of $C_p(\cdot)$. Chapter 2 of Magdi Ragheb and Adam M. Ragheb's book *Fundamental and Advanced Topics in Wind Power*, along with the aforementioned texts being used for system modeling describe this as the *Betz Limit*. This limit provides that a wind turbine can extract, at most 59.2% of the mechanical energy available in a wind resource. However, non-ideal behavior result in systems which perform below this limit, typically closer to 40% [5, 9, 10]. A plot of λ against $C_p(\cdot)$ yields a curve, typically similar to the given in Fig. 2.2., from which the max power coefficient $C_{p,max}$ can be obtained. The tip speed ratio corresponding to the highest efficiency is known as the optimal tip speed ratio λ_o [9].

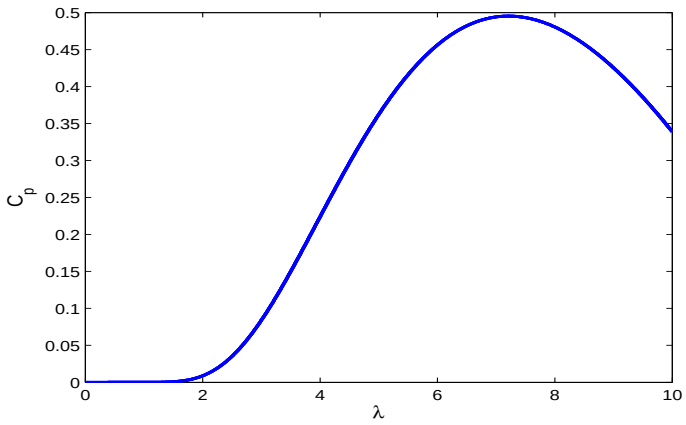

Figure 2.2: C_p v.s. λ Curve

2.2 Drive Train Dynamics

Rotational motion of the electrical generator is provided by rotational motion of the turbine rotor through a mechanical transmission. Known as a *drive train*, the structure of the transmission depends on the type of generator being used. Most systems employing induction generators use gearboxes with multiplying ratios in order to increase the rotational speed transmitted to the generators. Multi-pole synchronous machines however use what is known as a direct drive transmission, or more simply the direct coupling of the generator and the turbine rotor on the same shaft. This topology helps to eliminate inefficiency associated with weight and reliability of the gearbox [5].

In order to model the transmission of turbine rotor motion into generator rotation rigid drive train modeling will be used. Fig. 2.5, represents this topology. Since the generator to be modeled is synchronous in nature, the drive train ratio $1:1$. The rotational speed of the generator shaft, often known as the high speed shaft in cases where the drive train ratio results in a step up in generator speed, will be known as ω_r. For which the equation governing speed is $\omega_r = i \cdot \omega_l$, where i is the drive train ratio, and ω_l is the rotational speed from the low speed shaft, or that created by rotation of the turbine. The drive train dynamics in terms of the inertias are as follows:

$$J_h \frac{d\omega_r}{dt} = \frac{\eta}{i}\tau_m - \tau_e \tag{2.3}$$

$$J_l \frac{d\omega_l}{dt} = \tau_m - \frac{i}{\eta}\tau_e, \tag{2.4}$$

where η is the efficiency of transmission, and τ_e is the electromagnetic torque induced in the generator.

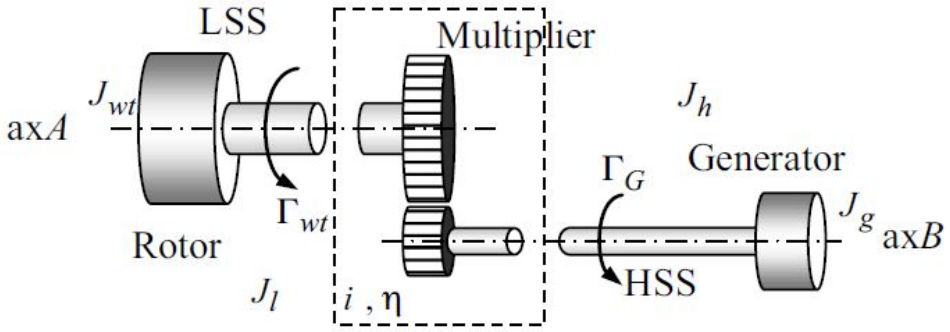

Figure 2.3: Rigid Drive Train

Due to the direct coupling, $i = 1$ and η will be considered to be 100%. This will mean that J_h is simply $-J_l$. Letting $J = J_h$ be the drive train inertia, and considering the stiffness coefficient B the resulting equation governing the behavior of the drive train can be reduced to a single equation:

$$\frac{d\omega_r}{dt} = \frac{\tau_m}{J} - \frac{\tau_e}{J} - \frac{B\omega_r}{J}. \tag{2.5}$$

The stiffness coefficient is typically of a small value, and is often neglected for simplicity. However, in this work the complexity added by its inclusion is negligible, and therefore it will be considered.

2.3 Permanent Magnet Synchronous Generator Modeling

The voltage equations for a synchronous generator, as provided by the IEEE standard for synchronous generator modeling [11] are given as

$$\begin{bmatrix} v_a \\ v_b \\ v_c \\ e_f d \end{bmatrix} = \begin{bmatrix} R_a & 0 & 0 & 0 \\ 0 & R_b & 0 & 0 \\ 0 & 0 & R_c & 0 \\ 0 & 0 & 0 & R_{fd} \end{bmatrix} \begin{bmatrix} -i_a \\ -i_b \\ -i_c \\ i_{fd} \end{bmatrix} + \frac{d}{dt} \begin{bmatrix} \Psi_a \\ \Psi_b \\ \Psi_c \\ \Psi_{fd} \end{bmatrix}. \tag{2.6}$$

The terms for (2.6) are defined within Table 2.1. Taking into acount the construction of a

Armature Winding Voltages:	v_a, v_b, v_c
Field Voltage:	e_{fd}
Armature phase resistance:	$R_a, R_b R_c$
Field-winding resistance:	R_{fd}
Winding currents:	i_a, i_b, i_c, i_{fd}
Winding Flux Linkage:	$\Psi_a, \Psi_b, \Psi_c, \Psi_{fd}$

Table 2.1: Generator Parameters

PMSG, the field-winding equation can be neglected. It then follows that the flux linkages for the various phases are given as

$$\Psi_a = L_{aa} i_a + L_{ab} i_b + L_{ac} i_c \tag{2.7}$$

$$\Psi_b = L_{ab} i_a + L_{bb} i_b + L_{bc} i_c \tag{2.8}$$

$$\Psi_c = L_{ac} i_a + L_{bc} i_b + L_{cc} i_c. \tag{2.9}$$

$$\tag{2.10}$$

The inductances given in (2.8) through (2.10) are deifned within Table 2.2. By means

Armature-phase self inductances:	L_{aa}, L_{bb}, L_{cc}
armature phase-phase mutal inductances:	L_{ab}, L_{bc}, L_{ac}

Table 2.2: Armature Inductances

of the Park's transformation technique the stationary stator reference frame (a, b, c) coordinate model of a synchronous generator can be converted to the stationary rotor $(d, q, 0)$ coordinate model of a PMSG [5, 9, 11, 12].

The simplified matrix representation of (2.6); disregarding field winding effects can be

given as

$$\mathbf{V}_{abc} = \mathbf{R}_{ss} \cdot \mathbf{I}_{abc} + \frac{d}{dt}(\mathbf{L}_{ss} \cdot \mathbf{I}_{abc}), \tag{2.11}$$

where the matrix $\mathbf{R}_{ss}$ represents the armature-phase resistances, and the armature-phase self and mutual inductances are given by

$$\mathbf{L}_{ss} = \begin{bmatrix} L_{aa} & L_{ab} & L_{ac} \\ L_{ab} & L_{bb} & L_{bc} \\ L_{ac} & L_{bc} & L_{cc} \end{bmatrix}. \tag{2.12}$$

From the Park's transform, it follows that the transformation matrix

$$\mathbf{T} = \frac{2}{3} \begin{bmatrix} cos(\sigma) & cos(\sigma - \frac{2\pi}{3}) & cos(\sigma - \frac{4\pi}{3}) \\ -sin(\sigma) & -sin(\sigma - \frac{2\pi}{3}) & -sin(\sigma - \frac{4\pi}{3}) \\ \frac{1}{2} & \frac{1}{2} & \frac{1}{2} \end{bmatrix}, \tag{2.13}$$

where σ represents the phase angle difference between the A-axis and the direct axis (d-axis) of the rotor. Application of the Park's transformation to find the direct, quadrature, and zero axis voltages, represented by $\mathbf{U}_{dq0}$ gives

$$\mathbf{T} \cdot \mathbf{V}_{abc} = \mathbf{T} \cdot \mathbf{R}_{ss} \cdot \mathbf{T}^{-1} \cdot \mathbf{T} \cdot \mathbf{I}_{abc} + \mathbf{T} \cdot \frac{d}{dt}(\mathbf{L}_{ss} \cdot \mathbf{I}_{abc}) \tag{2.14}$$

$$\mathbf{U}_{dq0} = \mathbf{T} \cdot \mathbf{R}_{ss} \cdot \mathbf{T}^{-1} \cdot \mathbf{I}_{dq0} + \mathbf{T} \cdot \frac{d}{dt}(\mathbf{T} \cdot \mathbf{\Lambda}_{dq0}), \tag{2.15}$$

where the $dq0$ flux linkage, and the time derivatives are

$$\mathbf{\Lambda}_{dq0} = \mathbf{T} \cdot \mathbf{\Lambda}_{abc} = \mathbf{T} \cdot \mathbf{L}_{ss} \cdot \mathbf{I}_{abc} \tag{2.16}$$

$$\dot{\mathbf{\Lambda}}_{dq0} = (\mathbf{T} \cdot \mathbf{L}_{ss} \cdot \mathbf{T}^{-1}) \cdot \mathbf{I}_{dq0}. \tag{2.17}$$

Next, note that $\frac{d}{dt}(\mathbf{T}) = \omega_e \mathbf{G} \cdot \mathbf{T}$ where

$$\mathbf{G} = \begin{bmatrix} 0 & 1 & 0 \\ -1 & 0 & 0 \\ 0 & 0 & 0 \end{bmatrix} \tag{2.18}$$

and ω_e is the developed generator electrical angular frequency [5]. It then follows that

$$\mathbf{U}_{dq0} = \mathbf{T} \cdot \mathbf{R}_{ss} \cdot \mathbf{T}^{-1} \cdot \mathbf{I}_{dq0} + \dot{\mathbf{\Lambda}}_{dq0} - \omega_e \mathbf{G} \cdot \mathbf{\Lambda}_{dq0}. \tag{2.19}$$

However, from

$$\dot{\mathbf{\Lambda}}_{dq0} = (\mathbf{T} \cdot \mathbf{T}^{-1}) \cdot \dot{\mathbf{I}}_{dq0}, \tag{2.20}$$

it can be noted that $\mathbf{T} \cdot \mathbf{L}_{ss} \cdot \mathbf{T}^{-1}$ is time independent. Therefore

$$\mathbf{U}_{dq0} = \mathbf{R}_{ss} \cdot \mathbf{I}_{dq0} + (\mathbf{T} \cdot \mathbf{L}_{ss} \cdot \mathbf{T}^{-1}) \cdot \dot{\mathbf{I}}_{dq0} - \omega_e \mathbf{G} \cdot (\mathbf{T} \cdot \mathbf{L}_{ss} \cdot \mathbf{T}^{-1}) \cdot \mathbf{I}_{dq0} \tag{2.21}$$

Let the time invariant direct, quadrature, and zero axis inductance matrix be defined as

$$\mathbf{L}_{dq0} = \mathbf{T} \cdot \mathbf{L}_{ss} \cdot \mathbf{T}^{-1} = \begin{bmatrix} L_d & 0 & 0 \\ 0 & L_q & 0 \\ 0 & 0 & L_0 \end{bmatrix} \tag{2.22}$$

Lastly, simplification results in the expanded state space $(d, q, 0)$ voltage equations which are given as

$$\begin{bmatrix} u_d \\ u_q \\ u_0 \end{bmatrix} = \begin{bmatrix} R_s & 0 & 0 \\ 0 & R_s & 0 \\ 0 & 0 & R_s \end{bmatrix} \begin{bmatrix} i_d \\ i_q \\ i_0 \end{bmatrix} + \begin{bmatrix} 0 & -\omega_e L_q & 0 \\ \omega_e L_d & 0 & 0 \\ 0 & 0 & 0 \end{bmatrix} \begin{bmatrix} i_d \\ i_q \\ i_0 \end{bmatrix} + \begin{bmatrix} L_d & 0 & 0 \\ 0 & L_q & 0 \\ 0 & 0 & L_0 \end{bmatrix} \begin{bmatrix} \frac{di_q}{dt} \\ \frac{di_q}{dt} \\ \frac{di_0}{dt} \end{bmatrix} \tag{2.23}$$

The final representation for the direct-axis (d-axis) and the quadrature-axis(q-axis) voltages, matching models given in various sources including [5, 9, 11, 12] to be used within this work becomes:

$$u_d = R_s i_d + L_d \frac{di_d}{dt} - L_q i_q \omega_e \tag{2.24}$$

$$u_q = R_s i_q + L_q \frac{di_q}{dt} + (L_d i_d + \Psi_m)\omega_e, \tag{2.25}$$

Considering a surface mounted PMSG, one in which the rotor makes use of surface mounted permanent magnets [13], will result in the inductances L_q and L_d having the

same value, and therefore$L_d = L_q = L$ [5]. Using this consolidation, and rearranging (2.24) and (2.25) to form the system to be controlled results in the following:

$$\frac{di_d}{dt} = -\frac{R_s}{L} i_d + \omega_e i_q - \frac{1}{L} u_d \tag{2.26}$$

$$\frac{di_q}{dt} = -\frac{R_s}{L} i_q - \omega_e i_d - \frac{1}{L} u_q + \frac{1}{L} \Psi_m \omega_e \tag{2.27}$$

CHAPTER 3

SLIDING MODE CONTROL

3.1 Introduction

One of the control systems techniques applied to the VS-WECS model that has been developed is sliding mode control (SMC). According to [14], it is in the control of hybrid dynamical systems with both discontinuous and continuous behavior that sliding mode control (SMC) made it's debut. Eventually sliding modes became a principal mode of operation for these variable-structure systems. Nearly all variable-structure design methods purposefully introduce sliding modes. The commonly touted benefits of SMC continue to make it a popular topic of study among control systems engineers. Among the benefits offered by SMC are order reduction, low sensitivity, and efficiency in controlling complex high-order and even nonlinear systems [14, 15, 16]. It is generally desirable to decouple a system's motion into individual components in order to simplify the study of multi-dimensional systems. Enforcement of sliding modes enables this order reduction. This leads to decoupling, and subsequent simplification of the design process. The discontinuous function employs high-frequency switching. Theoretically, this switching is infinite. Modern semi-conductor devices make this high-frequency control action attainable, but the effects of switching delays needs to compensated for. This switching action sees uses in suppression of external disturbances, and uncertainties in model parameters. These finite switching actions, unlike continuous high-gain control systems, make this invariance of state behavior achievable [14]. In SMC state trajectories are forced to reach a sliding manifold or sliding surface within a finite amount of time. Then, the trajectories are to remain at this manifold for all future time. Also, matched uncertainties do not affect the motion along this surface [17].

3.2 Outline of Sliding Mode Control Methodology

Consider systems described by nonlinear, or affine differential equations of the form:

$$\dot{x} = f(x, t, u) \tag{3.1}$$

in an arbitrary n-dimensional space, with m-dimensional vector control actions, where $x \in \Re^n, f \in \Re^n, u \in \Re^m$, and t represents time. The control is selected as

$$u_i = \begin{cases} u_i^+(x,t) & s_i(x) > 0 \\ u_i^-(x,t) & s_i(x) < 0 \end{cases} \quad (i = 1, ..., m) \tag{3.2}$$

The control is a station function which is discontinuous. Each component u_i can experience discontinuities on $s_i(x) = 0$. $s_i(x) = 0$ are continuous nonlinear surfaces in the state space. $u_i^+(x,t)$ and $u_i^-(x,t)$ are continuous and do not equal each other [14].

Sliding modes may occur at the intersection of m-surfaces $s_i(x) = 0, (i = 1, ..., m)$, and the order of the motion equations is m less than the original order of the system. The discontinuous function uses high (theoretically infinite) gain. This is a common tool for the suppression of disturbances and parameter uncertainties in a system. This organization results in order reduction of the system, and invariance to parameter uncertainties and disturbances [14].

3.3 Regularization

Most conventional mathematical techniques for the solution of continuous differential equations are not applicable for discontinuous control methods such as SMC. One of the broadest methods requires that the Lipschitz condition $||f(x_1) - f(x_2)|| < L||x_1 - x_2||$ is satisfied by functions $f(x)$ in the right-hand sides of the differential equation. L is positive number known as the Lipschitz constant, and x_1 and x_2 are any point.This constrains the growth of the function to be less than that of some linear function, as long as x_1 and x_2 are not close to the discontinuity point [14]. However, the boundary layer

method of regularization can more effectively deal with more expansive scope of non ideal conditions. The boundary layer method can be described through consideration of the following general system with a vector control:

$$\dot{x} = f(x,u) \quad x, f \in \Re^n,\ u(x) \in \Re^m \tag{3.3}$$

$$u(x) = \begin{cases} u_i^+(x,t) & s_i(x) > 0 \\ u_i^-(x,t) & s_i(x) < 0 \end{cases}$$

where for the vector $s(x)$, it's components $[s_1(x)...s_m(x)]$ are smooth functions. The ith component of $u(x)$ experiences discontinuities on the ith surface $s_i(x) = 0$. Sliding modes may occur at $s(x) = 0$. In order to obtain the sliding mode equations, the control $\tilde{u}$ replaces the ideal control given the for (3.3), such that the solution exists in the broadest sense. The boundary layer, with width $\Delta > 0$ confines the trajectories, such that they are not bound to $s(x) = 0$ only. It follows that:

$$||s(x)|| \leq \Delta, \quad ||s|| = (s^T s)^{1/2}.$$

The boundary layer regularization method can be summarized as follows: for the approximation of the control $u = \tilde{u}$, and a boundary layer width Δ which asymptotically approaches zero, if the limit of the solution of (3.3) exists such that

$$\lim_{\delta \to 0} x(t, \Delta) = x^*(t), \tag{3.4}$$

then $x^*(t)$ represents the solution with ideal sliding mode [14], as shown by Fig.3.1 [18].

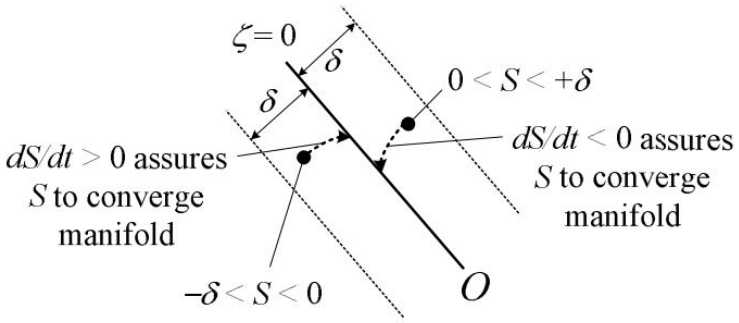

Figure 3.1: State Behavior Along Switching Surface

3.4 Equivalent Control Method

The equivalent control method is another important concept in SMC, and attempts to analyze whether the equations can be taken as the motion model. The initial state vector of the system (3.3) is assumed to lie apart from the sliding surface. Through satisfying the reaching conditions, the state reaches the sliding surface. The equivalent control is responsible for the motion of the state along the sliding surface, towards the origin [14, 18].

To begin, the control discontinuities are disregarded, and the vector u is calculated such that it's time derivative

$$\dot{s}(x) = \frac{\partial s}{\partial x} \cdot f(x, u) = 0. \tag{3.5}$$

Substitute the equivalent control u_{eq} for the discontinuous control u into the original system (3.3):

$$\dot{x} = f(x, u_{eq}) \tag{3.6}$$

where u_{eq} is a continuous function, and is a solution that exists for (3.5). Note that for initial conditions $s\big(x(0)\big) = 0$, agreeing with (3.5), further motion is dictated by (3.6), and is along the state trajectories in manifold $s(x) = 0$, as in the sliding mode for (3.3). (3.6) is considered the sliding mode equation where m discontinuity surfaces $s_i(x) = 0 (i = 1, ..., m)$ intersect [14].

For input-affine systems with right-hand sides in the motion equations (3.3) as linear functions of the control input u:

$$\dot{x} = f(x) + B(x)u \quad x, f(x) \in \Re^n,\ B(x) \in \Re^{n \times m},\ u(x) \in \Re^m \tag{3.7}$$

$$u_i(x) = \begin{cases} u_i^+(x,t) & s_i(x) > 0 \\ \\ u_i^-(x,t) & s_i(x) < 0 \end{cases}.$$

Similarly, for control component u_i, each surface $s_i(x) = 0$, is the set of discontinuity points. First select the following Lyapunov candidate, and its corresponding derivative:

$$V = \frac{1}{2} s^T s \tag{3.8}$$

$$\dot{V} = \frac{\partial V}{\partial s} = s^T \cdot \dot{s}, \tag{3.9}$$

where

$$\dot{s} = \frac{\partial s}{\partial x}\dot{x} = \frac{\partial s}{\partial x}\big(f(x) + B(x)u\big). \tag{3.10}$$

Therefore, in order to ensure that the state trajectories are driven towards the switching surface, the control u_{eq} must be chosen such that $\dot{V} < 0$. The equivalent control is given as follows:

$$u_{eq} = -(G(x)B(x))^{-1}G(x)f(x) \tag{3.11}$$

where $m \times n$ matrix $G = \partial s/\partial x$ [18]

The purpose of the equivalent control is due to the fact that motion in sliding mode was considered somewhat ideal. Realistic imperfections in switching devices result in state oscillations about the sliding manifold, instead of the state velocity vector being oriented precisely along it. The oscillations are made up of high-frequency and slow components. The equivalent control represents the slow component of the control. The equivalent control depends on system parameters, and helps ensure that the state is always driven towards the sliding manifold, while the switching control keeps the state trajectory bound to a certain area around it [14].

3.5 Switching Control

Mathematically, the switching portion of the control can be represented various ways. Two such ways are the signum and hysteresis functions. The signum function is the

method of choice in this work, which is given by

$$sgn(s) = \begin{cases} 1, & \text{if } s > 1 \\ 0, & \text{if } s = 0 \\ -1, & \text{if } s < 1. \end{cases} \tag{3.12}$$

This switching control is mathematically ideal, and lends itself to simpler calculations. However, high frequency switching devices will ultimately experience switching delay, making its behavior better categorized by a hysteresis. This has the effect of allowing the state trajectory to shoot past the sliding surface. This behavior is colloquially referred to as *chattering*. Fig. 3.2 represents this effect [18].

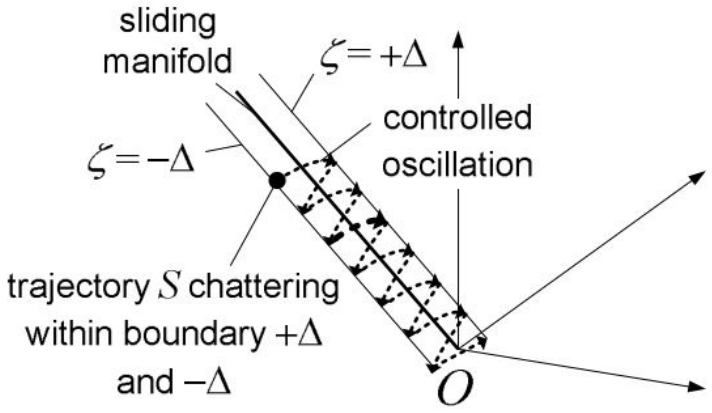

Figure 3.2: Trajectory Behavior Due to Switching Delays

3.6 Existence Conditions

For nonlinear systems of the form (3.7), existence conditions can be derived though analysis of the stability of the motion projection on subspace s governed by the differential equation

$$\dot{s} = \frac{\partial s}{\partial x} \cdot \frac{\partial x}{\partial t}. \tag{3.13}$$

Subsequently the control is re-written as

$$u(x) = u_{eq}(x) + u_0(x) sgn(s), \tag{3.14}$$

It follows that on subspace s, the motion projection is governed by

$$\dot{s} = \frac{\partial s}{\partial x}\big(f(x) + B(x)(u_{eq} + u_N)\big), \tag{3.15}$$

where $u_N = u_0 sgn(s)$. Standard analysis techniques for stability analysis of affine systems involve trying to find a candidate Lyapunov function. In order to find the existence conditions conditions for stability of the origin $s = 0$ for equation (3.15), this standard nonlinear analysis approach is used. However, given the discontinuous nature of the right-hand side of the motion equation, and that the motion equation is undefined when the argument of the switching function is zero, care must be taken [14].

The discontinuous components of control should be replaced by their corresponding equivalent ones in order to be able to use a Lyapunov function in the form of the sum of absolute values. Then, the time derivative of the Lyapunov function should be found. The following definition, theorem, and remarks from [14] are necessary in order to facilitate this design process.

Definition 3.1. The set $S(x)$ in the $s(x) = 0$ is the domain of the sliding mode if, for the motion governed by equation (3.15), the origin in the subspace s is asymptotically stable with finite convergence time for each x from $S(x)$.

Definition 3.2. If the inequalies

$$\lim_{s \to +0} \dot{s} < 0 \tag{3.16}$$

$$\lim_{s \to -0} \dot{s} > 0 \tag{3.17}$$

holds for any x, then it is simultaneously the condition for the state to reach the sliding manifold from any initial point. This is also known as the reaching or reachability condition.

These definitions deal solely with time-invariant systems. However, the results remain valid for time -varying systems. The primary difference is that for a time-varying sliding

manifold $s(x,t) = 0$, the equivalent control equation should contain the addition of $\delta s(x,t)/\delta t$ term:

$$\dot{s} = Gf + GBu_{eq} + \partial s(x,t)/\partial t = 0$$

and it's solution $u_{eq} = -(GB)^{-1}(Gf + \partial s/\partial t)$ should be substituted into (3.7) regardless of whether the motion equation functions f and B are time dependent [14]

3.7 Relevant Applications

Recent publications continue to research into the application of SMC in a range of topics. Some range from pure control systems theoretical expansion [15, 19] to model applications [16, 20, 21, 22]. The primary focus of this work is in the context of electromechanical energy conversion for permanent magnet synchronous machines. So, the application precedents given primarily concern these types systems. However, it should be noted that work in other electric machines and drives such as induction machines has also received a notable amount of attention. In WECS, research into these generation means, demonstrated in works such as [23, 24, 25], shows the . Coinciding and expanding upon theory laid forth in [14], detailed coverage of permanent magnet synchronous motor (PMSM) control appears in [16, 20]. These two works focus on speed control, but the given simulations and implementations demonstrate the high level of control and robustness that SMC offers in the control of electric machines. As stated previously, the increased use of PMSGs in wind energy applications has created the need for more powerful control systems designs. Research such as, but not limited to that given in [21] and [22] demonstrates the effectiveness of this control systems technique in speed control of PMSG based VS-WECS control. Current control schemes such as those in [26] also demonstrate promising results.

CHAPTER 4

CONTROL USING LINEAR MATRIX INEQUALITIES WITH VARIOUS PERFORMANCE CRITERIA

4.1 Introduction

The study of linear matrix inequalities (LMIs) dates back to the 1940's, with use in control systems research following in the 1960's [27]. LMI research within control systems theory demonstrated the ability to solve convex control systems. However, the tedious nature of the solutions prevented any practical use in complex systems [28]. In the the following decades advancements in computing, and the development of powerful solution techniques helped to further the practical use of LMIs in complex systems control applications [27, 28].

Control systems research involving the use of LMIs consistently demonstrates effectiveness in an assortment of potential engineering applications. Power systems research into load frequency control in systems with communication delays, and robust controllers for multi-machine systems help to provide practical examples of applicability [29, 30]. The primary distinguishing factor between these works appears in the performance goals for which each controller is designed.

Finite-time stability (FTS) and finite-time boundedness (FTB), concepts concerning the stability of a state of a system in the presence of L_2 type disturbances during a finite time interval given initial state values, receive extensive attention in the various works of Amato, et. al. Methods for control and stability using the solutions of LMIs designed with FTS or FTB performance criteria consistently demonstrate promise in applications for various system types including, but not restricted to linear time varying systems, discrete-time linear systems, nonlinear quadratic systems, dynamic output feedback, and linear systems with parametric uncertainties [31, 32, 33, 34, 35].

In the 1970's, robust control theory surfaced with the primary goal of controlling systems with parametric uncertainties. Within robust control, H_2 and H_∞ techniques receive a significant amount of focus in research and publication [36]. LMI control research involving robust H_∞ performance criteria applied to continuous-time nonlinear controller demonstrates novel effectiveness when applied to a model of an inverted pendulum [37]. Electric machine and helicopter control research demonstrate the effectiveness of designs in both power systems and aerospace, when employing LMI based control techniques with H_∞ performance criterion [38, 39].

4.2 General System Modeling

The following gives the conditions for a general system with disturbances, to be used in the definitions of the performance criteria.

Let the continuous-time system of interest be the time-invariant continuous-time system given by

$$\begin{aligned} \dot{x} =& F(x,u,w) = (A+\Delta A)x \\ &+(B+\Delta B)u + (F+\Delta F)w \end{aligned} \tag{4.1a}$$

$$\dot{w} = \Phi w. \tag{4.1b}$$

where $x \in \Re^n$ is the state of the system, $u \in \Re^m$ is the input applied to the system, and $w \in \Re^q$ is a structured disturbance. A, B, F, and Φ are the known coefficient matrices of appropriate dimensions, and $\Delta A, \Delta B$, and ΔF are bounded fluctions in the systems parameters. The corresponding controlled output is

$$z = Cx + Du, \tag{4.2}$$

where, C and D are known coefficient matrices. The bounded L_2 type disturbances are

defined as

$$\Delta A \Delta A^T \leq \sigma_A^2 I \tag{4.3}$$

$$\Delta B \Delta B^T \leq \sigma_B^2 I \tag{4.4}$$

$$\Delta F \Delta F^T \leq \sigma_F^2 I. \tag{4.5}$$

Let the control u be a linear state feedback controller with gain $K \in \Re^{n \times m}$ be denoted as

$$u = Kx. \tag{4.6}$$

For discrete-time, the system will be given as follows: The general system discrete-time dynamics, disturbance, controlled output, and input are adapted from the continuous time system given previously by (4.1a), (4.1b), (4.2), and (4.6)

$$x_{k+1} = (A + \Delta A)x_k + (B + \Delta B)u_k + (F + \Delta f)w_k \tag{4.7a}$$

$$w_{k+1} = \phi w_k, \tag{4.7b}$$

$$z_k = Cx_k + Du_k \tag{4.7c}$$

$$u_k = Kx_k. \tag{4.7d}$$

With parameter definitions equivalent to those in the continuous-time system.

4.3 Finite-Time Boundedness

What follows are the definitions of finite time boundedness as used in this work, as well as an important Lemma to be used in the control design to follow for both continuous-time and discrete-time cases.

Definition 4.1. The following extends from the definitions for short-time stability, or equivalently FTS, and FTB given by [40] and [34] to equations (4.1a) and (4.1b). For the continuous-time case, given the positive scalars α_x^2, α_w^2, and T, and matrix $R > 0$, the

system is FTB with regards to (T, R), if $\forall\ t \in [0, T]$

$$\begin{cases} x(0)^T R x(0) \leq \alpha_x^2 \\ w(0)^T w(0) \leq \alpha_w^2 \end{cases} \Rightarrow x(t)^T R x(t) \leq \beta^2.$$

The discrete-time definition of FTB (4.1) extends from [41], and is given as follows:

Definition 4.2. The system $x_{k+1} = Ax_k + Fw_k$ where $k \in \mathbb{N}_0$, and $w_{k+1} = \phi w_k$ is FTB with respect to $(\alpha_x, \alpha_w, R, N)$, where matrix $R > 0$, $0 \leq \alpha_x \leq \beta$, $\alpha_w \geq 0$, and $N \in \mathbb{N}_0$, if

$$\begin{cases} x_0^T R x_0 \leq \alpha_x^2 \\ w_0^T w_0 \leq \alpha_w^2 \end{cases} \Rightarrow x_k^T R x_k \leq \beta^2 \quad \forall k \in 1, ..., N.$$

The following Lemma provides sufficient conditions for continuous-time FTB

Lemma 4.3. *Given the system dynamics in equations (4.1a), (4.1b), and (4.2) the FTB condition can be satisfied if there exists matrices, $P_1 > 0$ and $P_2 > 0$, such that the following condition holds:*

$$\lambda_{min}(P_1)\beta^2 \leq [\lambda_{max}(P_1)\alpha_x^2 + \lambda_{max}(P_2)\alpha_w^2]e^{\alpha t} \tag{4.8}$$

where the minimum and maximum eigenvalues of the argument are represented $\lambda_{min}(\cdot)$ and $\lambda_{max}(\cdot)$ respectively.

Proof. Consider further the quadratic Lyapunov function

$$V\big(x(t), w(t)\big) = x(t)^T P_1 x(t) + w(t)^T P_2 w(t), \tag{4.9}$$

with the corresponding inequality found in [17]:

$$\dot{V}\big(x(t), w(t)\big) < \alpha V\big(x(t), w(t)\big). \tag{4.10}$$

Divide both sides of (4.9) by $V(x(t), w(t))$, and integrate from from 0 to t, where $t \in [0, T]$ to obtain the following inequality:

$$ln\frac{V\big(x(t), w(t)\big)}{V(x(0), w(0))} < \alpha t. \tag{4.11}$$

From (4.9) re-write the energy function as

$$\begin{bmatrix} x(t)^T & w(t)^T \end{bmatrix} \begin{bmatrix} P_1 & 0 \\ 0 & P_2 \end{bmatrix} \begin{bmatrix} x(t) \\ w(t) \end{bmatrix}. \tag{4.12}$$

Before continuing, denote

$$\zeta = \begin{bmatrix} x(t) \\ w(t) \end{bmatrix}. \tag{4.13}$$

Combining (4.11), (4.12), and (4.13), and considering inequality 4.10 it follows that:

$$\zeta(t)^T \begin{bmatrix} P_1 & 0 \\ 0 & P_2 \end{bmatrix} \zeta(t) < \zeta(0)^T \begin{bmatrix} P_1 & 0 \\ 0 & P_2 \end{bmatrix} \zeta(0) e^{\alpha T}. \tag{4.14}$$

Subsequently

$$\zeta(t)^T \begin{bmatrix} P_1 & 0 \\ 0 & P_2 \end{bmatrix} \zeta(t) = x(t)^T P_1 x(t) + w(t)^T P_2 w(t), \tag{4.15}$$

which satisfies

$$x(t)^T R x(t) \leq \beta^2 \tag{4.16}$$

from the definition for FTB. Then, denote the following matrices M and P as:

$$M = \begin{bmatrix} R^{\frac{1}{2}} & 0 \\ 0 & I \end{bmatrix}, P = \begin{bmatrix} P_1 & 0 \\ 0 & P_2 \end{bmatrix}.$$

For inequality (4.14) replace P, and pre- and post-multiply by M to obtain

$$\zeta(t)^T MPM\zeta(t) < \zeta(0)^T MPM\zeta(0) e^{\alpha t}. \tag{4.17}$$

Using Rayleigh's inequality

$$\lambda_{min}(R) u^T u < u^T R u < \lambda_{max}(R) u^T u, \tag{4.18}$$

and (4.15) it follows that from the left side of (4.16),

$$\begin{aligned} \zeta(t)^T MPM\zeta(t) &= x(t)^T R^{\frac{1}{2}} P_1 R^{\frac{1}{2}} x(t) + w(t)^T P_2 w(t) \\ &\geq \lambda_{min}(P_1) x(t)^T R x(t) = \lambda_{min}(P_1) \beta^2, \end{aligned} \tag{4.19}$$

Considering the right side of (4.8), the matrix P, and the following:

$$\begin{cases} x_0^T R x_0 \leq \alpha_x^2 \\ w_0^T w_0 \leq \alpha_w^2 \end{cases},$$

from the definition for FTB it follows that

$$\begin{aligned} &\zeta(0)^T M P M \zeta(0) e^{\alpha t} \\ &= [x(0)^T R^{\frac{1}{2}} P_1 R^{\frac{1}{2}} x(0) + w(0)^T P_2 w(0)] e^{\alpha t} \\ &\leq [\lambda_{max}(P_1)\alpha_x^2 + \lambda_{max}(P_2)\alpha_w^2] e^{\alpha t}, \end{aligned} \tag{4.20}$$

Lastly, combine the (4.17) and (4.19) to achieve 4.8. □

Subsequently, the discrete-time case of this lemma follows from [41] as:

Lemma 4.4. *Given the system (4.7) the FTB condition can be satisfied with respect to* $(\alpha_x, \alpha_w, \beta, R, N)$*, if there exists matrices,* $P_1 > 0, P_2 > 0$*, and positive scalar* $\alpha < 1$*, such that the following condition holds:*

$$\lambda_{min}(R^{-1/2} P_1 R^{-1/2})\beta^2 < \alpha^k \lambda_{max} \begin{bmatrix} R^{-1/2} & 0 \\ 0 & P_2 \end{bmatrix} (\alpha_x^2 + \alpha_w^2) \tag{4.21}$$

.

Proof. Assume that $x_0^T R x_0 \leq \alpha_x^2$, and $w_0^T w_0 \leq \alpha_w^2$. If the conditions in the lemma hold, then $x_k^T R x_k < \beta^2$ for all $k = 1, ..., N$.

For $V_k = x_k^T P_1 x_k + w_k^T P_2 w_k$, let

$$V_{k+1} < \alpha V_k, \quad 0 < \alpha < 1. \tag{4.22}$$

Subsequently

$$x_{k+1}^T P_1 x_{k+1} + w_{k+1}^T P_2 w_{k+1} < \alpha(x_k^T P_1 x_k + w_k^T P_2 w_k). \tag{4.23}$$

It can be found that

$$V_k < \alpha^k V_0, \tag{4.24}$$

or equivalently

$$x_k^T P_1 x_k + w_k^T P_2 w_k < \alpha(x_0^T P_1 x_0 + w_0^T P_2 w_0) \tag{4.25}$$

Using Ralyeigh's inequality of the form $\lambda_{min}(P)x^T x < x^T P x < \lambda_{max}(P)x^T x$ it can be found that

$$\begin{aligned}
\lambda_{min}(R^{-1/2}P_2R^{-1/2})x_k^T R x_k &< x_k^T(P_1)x_k \\
&< \alpha^k(x_0^T R^{-1/2} P_1 R^{-1/2} x_0 + w_0^T P_2 w_0) \\
&< \alpha^k(\lambda_{max}(R^{-1/2}P_1R^{-1/2}x_0^T R x_0) + \lambda_{max}(P_2)w_0^T w_0)
\end{aligned} \tag{4.26}$$

Therefore, if

$$\lambda_{min}(R^{-1/2}P_1R^{-1/2})\beta^2 < \alpha^k(\lambda(R^{-1/2}P_1R^{-1/2})\alpha_x^2 + \lambda_{max}(P_2)\alpha_w^2), \tag{4.27}$$

this is the condition given by the lemma, and is written equivalently as

$$\lambda_{min}(R^{-1/2}P_1R^{-1/2})\beta^2 < \alpha^k \lambda_{max} \begin{bmatrix} R^{-1/2} & 0 \\ 0 & P_2 \end{bmatrix} (\alpha_x^2 + \alpha_w^2) \tag{4.28}$$

□

4.4 H_∞ Control Design

A popular control systems design tool for multi-variable systems, H_∞-optimization is a we research concept from robust control theory. For a relevant frequency response function, H_∞-optimization is essentially the minimization of the infinity norm. The H_∞ norm can be defined as

$$||G(s)||_\infty = \sup_{u(t)\neq 0} \frac{||y(t)||_2}{||u(t)||_2}, \tag{4.29}$$

with external input $u(t)$ and output $y(t)$ The space H_∞ is also know as the Hardy space. This space is comprised of of all fluctuations that are bounded an analytic in the right-half complex plane. This method of optimization has differences from the also popular H_2-optimization. However, the allowance of explicit inclusion of robustness constraints is an important property of H_∞-optimization [42].

Definition 4.5. The following H_∞ design method is adapted from [43]. Given the performance output (4.2), structured noise $w(t)$, and a positive constant γ, the objective

$$J = \int_0^\infty (z^T z - \gamma^2 w^T w) dt < 0 \tag{4.30}$$

must be minimized, such that

$$\frac{\int_0^\infty z^T z dt}{\int_0^\infty w^T w dt} < \gamma^2. \tag{4.31}$$

Subsequently, for the discrete-time system, the H_∞ performance objective has the following definition, given as an extension from the continuous-time definition.

Definition 4.6. Given the performance output from $u_k = Kx_k$, structured noise w_k, and positive constant γ. The objective

$$J = \sum_{k=0}^{N} (z_k^T z_k - \gamma^2 w_k^T w) < 0 \tag{4.32}$$

must be minimized, such that

$$\frac{z_k^T z_k}{w_k^T w_k} < \gamma^2 \tag{4.33}$$

Lemma 4.7. *The following inequality from [44] states that the following condition*

$$AB^T + BA^T \leq \alpha AA^T + \alpha^{-1} BB^T, \tag{4.34}$$

Proof.

$$(\alpha^{\frac{1}{2}} A - \alpha^{-\frac{1}{2}} B)(\alpha^{\frac{1}{2}} A - \alpha^{-\frac{1}{2}} B)^T \geq 0. \tag{4.35}$$

It also follows that by choosing:

$$A = \begin{bmatrix} a^T \\ 0 \end{bmatrix} \; and \; B = \begin{bmatrix} 0 \\ b^T \end{bmatrix}, \tag{4.36}$$

that the following inequality holds:

$$\begin{bmatrix} 0 & a^T b \\ b^T a & 0 \end{bmatrix} \leq \begin{bmatrix} \zeta a^T a & 0 \\ 0 & \zeta^{-1} b^T b \end{bmatrix}. \tag{4.37}$$

□

4.5 Control Using Linear Matrix Inequalities

4.5.1 Linear matrix inequalities

A summarized definition of linear matrix inequalities obtained from [28] follows:

A *strict* LMI takes the following form of a positive definite matrix:

$$F(x) \triangleq F_0 + \sum_{i=1}^{m} x_i F_i > 0, \ \forall u \in \Re^n, \tag{4.38}$$

for the given variable $x \in \Re^m$ and symmetric matricies $F_i = F_i^T \in \Re^{n \times n}$, $i = 0, ..., m$. The leading principal minors of $F(x)$ are positive, and therefore equivalent to a set of n polynomial inequalities. Note also that LMIs of the form $F(x) \geq 0$ are referred to as *nonstrict*

Considering only *strict* LMIs, $\{x|F(x) > 0\}$ is a convex set, or the the LMI given by (4.38) is a convex constraint on x. This form is capable of representing many convex constraints on x. The ability of Lyapunov inequalities to be cast in the form of an LMI is of particular interest in this work.

For diagonal matricies F_i, the LMI exists as a set of linear inequalities. Schur complements are used in order to obtain an LMI from nonlinear (convex) inequalities. Consider the LMI

$$\begin{bmatrix} Q(x) & S(x) \\ S(x)^T & R(x) \end{bmatrix} > 0, \tag{4.39}$$

where $Q(x) = Q(x)^T, R(x) = R(x)^T$, and $S(x)$ are nonlinearly dependent on x. The LMI (4.39) is equivalent to the set of affine inequalities $R(x) > 0$, $Q(x) - S(x)R(x)^{-1}S(x)^T > 0$.

The Lyapunov inequality is given as follows:

$$A^T P + PA < 0, \tag{4.40}$$

where the matrix $A \in \Re^{n \times n}$ is given, and the matrix $P = P^T$ is the variable. The inequality (4.40) can be written in the form of 4.38, where $P_1, ..., P_m$ is the basis for a

symmetric $n \times n$ matrices ($m = n(n+1)/2$). Let $F_0 = 0$ and $F_i = -A^T P_i - P_i A$.

4.5.2 Schur complements

From [45] schur complement as used in this work is defined as follows:

For symmetric matricies A and C, suppose that the quadratic function

$$f(x, y) = x^T A x + 2x^T B y + y^T C y \tag{4.41}$$

is convex in (x, y). Therefore

$$\begin{bmatrix} A & B \\ B^T & C \end{bmatrix} \geq 0 \tag{4.42}$$

If C is nonsingular, then the matrix

$$A - BC^{-1}B^T \tag{4.43}$$

is the *Schur complement* of C in matrix

$$\begin{bmatrix} A & B \\ B^T & C \end{bmatrix} \tag{4.44}$$

4.5.3 Relevant applications

A number of articles researching the use of LMI based control methodologies in wind energy systems exist. Work in H_2/H_∞ power system stabiliziers [46], robust control of wind systems with system parameter uncertainties [47], robust model predictive pitch and torque control [48], and fuzzy DC link control of WECS [49] are examples of these. There is still much work to be done in this field, and the customizeable nature of the performance objectives make LMI based control a potentially wide ranging technique.

CHAPTER 5

SLIDING MODE CONTROL DESIGN AND SIMULATION

This section builds upon existing SMC control designs developed for FOC of VS-WECS in [14]. In this work, the basis for permanent magnet synchronous motor current and speed control through SMC is developed. Typically, the two are considered separately. In this work both current control and speed control are implemented. The previously developed plants for shaft and the PMSG are considered. Subsequent development and simulation of the proposed control scheme follows, and provides a control structure that is robust given model uncertainties, and exhibits a high level of performance given a highly varying wind input.

5.1 System Model

For the application of SMC, the system to be controlled is from equations (2.5), (2.26), and (2.27). First considering that $\omega_e = \frac{P}{2}\omega_r$, where P is the number of stator poles. Furthermore, $\tau_e = K_t i_q$, where $K_t = \frac{3}{4}P\Psi_m$. The overall third-order model to be used in the following design become:

$$\frac{di_d(t)}{dt} = -\frac{R_s}{L}i_d(t) + \frac{P}{2}i_q(t)\omega_r(t) - \frac{1}{L}u_d(t) \tag{5.1}$$

$$\frac{di_q(t)}{dt} = -\frac{R_s}{L}i_q(t) - \frac{P}{2}\big(i_d(t) - \frac{\Psi_m}{L}\big)\omega_r(t) - \frac{1}{L}u_q(t) \tag{5.2}$$

$$\frac{d\omega_r(t)}{dt} = \frac{\tau_m}{J} - \frac{K_t i_q(t)}{J} - \frac{B\omega_r(t)}{J}. \tag{5.3}$$

5.2 Sliding Surfaces

The first part of the controller design will be to define the three sliding surfaces for each dynamical equation. The sliding modes for (5.1), (5.2), (5.3) respectively are,

$$s_d(t) = [i_d(t) - i_d^*(t)] = 0 \tag{5.4}$$

$$s_q(t) = [i_q(t) - i_q^*(t)] = 0 \tag{5.5}$$

$$s_{\omega_r}(t) = [\omega_r(t) - \omega_r^*(t)] = 0. \tag{5.6}$$

The reference values for each surface are represented by $i_d^*(t)$, $i_q^*(t)$, and $\omega_r^*(t)$ respectively. For the d-axis and due to the nature of FOC, $i_d^*(t) = 0$. The speed reference $\omega_r = i\frac{\lambda v}{R}$. Recall that i is the fixed drive train multiplying ratio [9]. The q-axis current reference will be developed as a result of the control law to be developed for equation (5.3).

5.3 Reachability Conditions

The reachability conditions for the sliding surfaces to ensure that the state trajectories will be driven towards their corresponding sliding surfaces are [14].

$$s_d(t)\dot{s}_d(t) < 0 \tag{5.7}$$

$$s_q(t)\dot{s}_q(t) < 0 \tag{5.8}$$

$$s_{\omega_r}(t)\dot{s}_{\omega_r}(t) < 0. \tag{5.9}$$

5.4 Parameter Variations

In order to appropriately compensate for the presence of un-modeled dynamics present in the system (5.1)-(5.3). The system variables will be represented as in Table 3.1 Where the parameter will be equal to its nominal value plus some bounded disturbance.

Stator Resistance:	$R_s = \hat{R}_s + \Delta R_s$
Inductance:	$L = \hat{L} + \Delta L$
Flux Linkage:	$\Psi_m = \hat{\Psi}_m + \Delta\Psi_m$
Mechanical Torque:	$\tau_m = \hat{\tau}_m + \Delta\tau_m$
Inertia:	$J = \hat{J} + \Delta J$
Stiffness:	$B = \hat{B} + \Delta B$

Table 5.1: System Parameters

5.5 Direct Axis Control Design

In order to develop the d-axis controller inequality (5.7) must be satisfied. Using equation (5.1), (5.7) can be re-written as:

$$\frac{s_d(t)}{L}\left[- R_s i_d(t) + \frac{P}{2} L i_q(t)\omega_r(t) - L u_d(t) - L\frac{di_d^*(t)}{dt}\right] < 0. \tag{5.10}$$

Next, the d-axis control law is denoted as:

$$u_d(t) = u_{d,eq}(t) + u_{d,N}(t), \tag{5.11}$$

where $u_{d,eq}(t)$ designates the equivalent controller and $u_{d,N}(t)$ designates the switching controller. From the nominal values of the system parameters the equivalent control is:

$$u_{d,eq}(t) = -\hat{R}_s i_d(t) + \frac{P}{2}\hat{L} i_q(t)\omega_r(t) - \hat{L}\frac{di_d^*(t)}{dt}. \tag{5.12}$$

Therefore, $\dot{s}_d(t)$ from inequality (5.10) becomes:

$$\dot{s}_d(t) = \frac{1}{\Delta L}\left[-\Delta R_s i_d(t) - \Delta L\left(\frac{di_d^*(t)}{dt} - \frac{P}{2} i_q(t)\omega_r(t)\right) - u_{d,N}(t)\right]. \tag{5.13}$$

Due to the bounded nature of the system parameter uncertainties, along with the variables $\frac{di_d^*(t)}{dt}$, $i_d(t)$, $i_q(t)$, and $\omega_r(t)$, there exists a positive constant u_do such that

$$u_{do}(t) > \left|-\Delta R_s i_d(t) + \Delta L\frac{P}{2} i_q(t)\omega_r(t) - \Delta L\frac{di_d^*(t)}{dt}\right|. \tag{5.14}$$

From this, the switching control is taken to be:

$$u_{d,N}(t) = -u_{do} sign(s_d(t)). \tag{5.15}$$

The resulting control law for the d-axis should ensure that the trajectory of $i_d(t)$ is driven towards the surface (5.4), and remains there in the presence of bounded disturbances.

5.6 Quadrature Axis Control Design

The same method used for the d-axis control design can be applied towards the q-axis design. Considering the reachability condition inequality (5.8), and re-writing it using the dynamics for the q-axis given by (5.2) yields

$$\frac{s_q(t)}{L}\left[-R_s i_q(t) - \frac{P}{2}(L i_d(t) - \Psi_m)\omega_r(t) - u_q(t) - L\frac{di_q^*(t)}{dt}\right] < 0. \tag{5.16}$$

Again, control law, this time for the q-axis, is written as as the sum of the equivalent and switching controls:

$$u_q(t) = u_{q,eq}(t) + u_{q,N}(t). \tag{5.17}$$

The equivalent control will be taken as

$$u_{q,eq}(t) = -\hat{R}_s i_q(t) + \frac{P}{2}(\hat{L} i_d(t) - \hat{\Psi}_m)\omega_r(t) - \hat{L}\frac{di_q^*(t)}{dt}. \tag{5.18}$$

Then, $\dot{s}_q(t)$, from inequality (5.16) becomes

$$\dot{s}_q(t) = \frac{1}{\Delta L}\left[-\Delta R_s i_q(t) - \frac{P}{2}(\Delta L i_d(t) - \Delta\Psi_m)\omega_r(t) - \Delta L\frac{di_q^*(t)}{dt} - u_{q,N}(t)\right]. \tag{5.19}$$

As before, due to the bounded nature of the uncertainties, and the aforementioned variables, there exists a positive constant u_{qo} such that

$$u_{qo}(t) > \left|-\Delta R_s i_q(t) - \frac{P}{2}(\Delta L i_q(t) + \Delta\Psi_m)\omega_r(t) - \Delta L\frac{di_d^*(t)}{dt}\right|, \tag{5.20}$$

which leads to the switching control:

$$u_{q,N}(t) = -u_{qo} sgn(s_q(t)). \tag{5.21}$$

The final result is a controller which should ensure that the trajectory of the quadrature axis current $i_q(t)$ will be driven towards the reference value $i_q^*(t)$ and remain there.

5.7 Rotational Speed Controller Design

Once more, applying the same approach used in the previous two subsections; this time for equation (5.3), the primary contribution of this work in SMC is developed. The inequality given by (5.9) must be satisfied. Re-stating $\dot{s}_{\omega_r}(t)$ using (5.3) and (5.6), the reachability condition for the rotational speed dynamics becomes

$$s_{\omega_r(t)}\left[\frac{\tau_m}{J} - \frac{K_t i_q(t)}{J} - \frac{B\omega_r(t)}{J} - J\frac{d\omega_r^*(t)}{dt}\right] < 0. \tag{5.22}$$

By selection of the q-axis current reference as the control variable, the control law is designated as

$$i_q^*(t) = i_{q,eq}^*(t) + i_{q,N}^*(t). \tag{5.23}$$

From the nominal parameter values, the equivalent control is written as

$$i_{q,eq}^*(t) = \frac{1}{K_t}\left[\hat{\tau}_m - \hat{B}\omega_r(t) - \hat{J}\frac{d\omega_r^*(t)}{dt}\right]. \tag{5.24}$$

From (5.22), and using the bounded model uncertainties, $\dot{s}_{\omega_r}(t)$ is re-written to yield

$$\dot{s}_{\omega_r}(t) = \frac{1}{J}\left[\Delta\tau_m - \Delta B\omega_r(t) - \Delta J\frac{d\omega_r^*(t)}{dt} - K_t i_{q,N}(t)\right]. \tag{5.25}$$

Once more, there exists a positive constant i_{qo}, such that:

$$i_{qo}(t) > \left|\frac{1}{K_t}\left[\Delta\tau_m - \Delta B - \Delta J\frac{d\omega_r^*(t)}{dt}\right]\right|, \tag{5.26}$$

from which the switching control $i_{q,N}^*(t)$ is

$$i_{q,N}^*(t) = -i_{qo}sgn(s_{\omega_r}(t)). \tag{5.27}$$

The desired result of this controller is that the control variable $i_q^*(t)$ is adjusted to accurately compensate for rotational speed changes based upon the wind input. This

reference value is then used by the q-axis controller to accurately compensate for the changes. The final result should give $C_p(\lambda)$ near or at the Betz limit calculated for the system with behavior that is consistent given model uncertainties and un-modeled dynamics.

5.8 Simulation and Results

The implementation of the wind input, VS-WECS and PMSG dynamics, and the developed SMC controllers to create a model of a VS-WECS system and control architecture in Simulink is represented by Fig. 5.1.

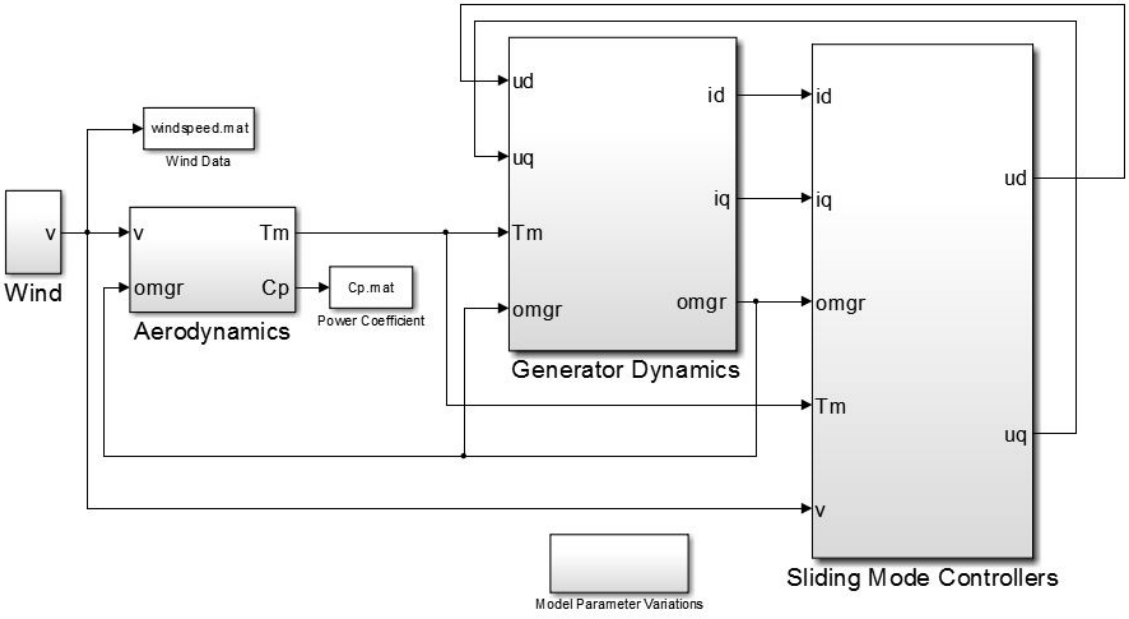

Figure 5.1: Global Simulink VS-WECS and SMC Model

Within each subsystem block the various parts of VS-WECS system are implemented with the certain parameter references generated through MATLAB files prior to simulation.

The nominal PMSG parameters used are listed in Table 3.2. Bounded parameter variations are implemented through the addition of bounded noise to each nominal parameter value within the Simulink model.

Rotor Radius:	$R_t = 3meters$
Stator Resistance:	$R_s = 3.5\Omega$
Inductance:	$L = 35mH$
Flux Linkage:	$\Psi_m = 0.3Wb$
Poles:	$P = 6$
Inertia:	$J = 1$
Stiffness:	$B = 0.001$

Table 5.2: Turbine and Generator Parameters

The following simulations demonstrate the performance of the controller given a range of wind inputs with varying degrees of intensity. The point of these simulations are to exhibit the high level of disturbance response, and reference tracking ability that the proposed controller can achieve.

5.8.1 Simulation 1: disturbance rejection

The purpose of the first simulation is to demonstrate the ability proposed control system design at steady state to cope with a drastic change in wind speed in a short amount of time, and then achieve a new steady state value. The wind profile used for this simulation is shown in Fig. 5.2. At the start of the simulation the wind has a constant velocity of seven meters per second. At time $t = 30$ seconds the wind jumps quickly to nine meters per second.

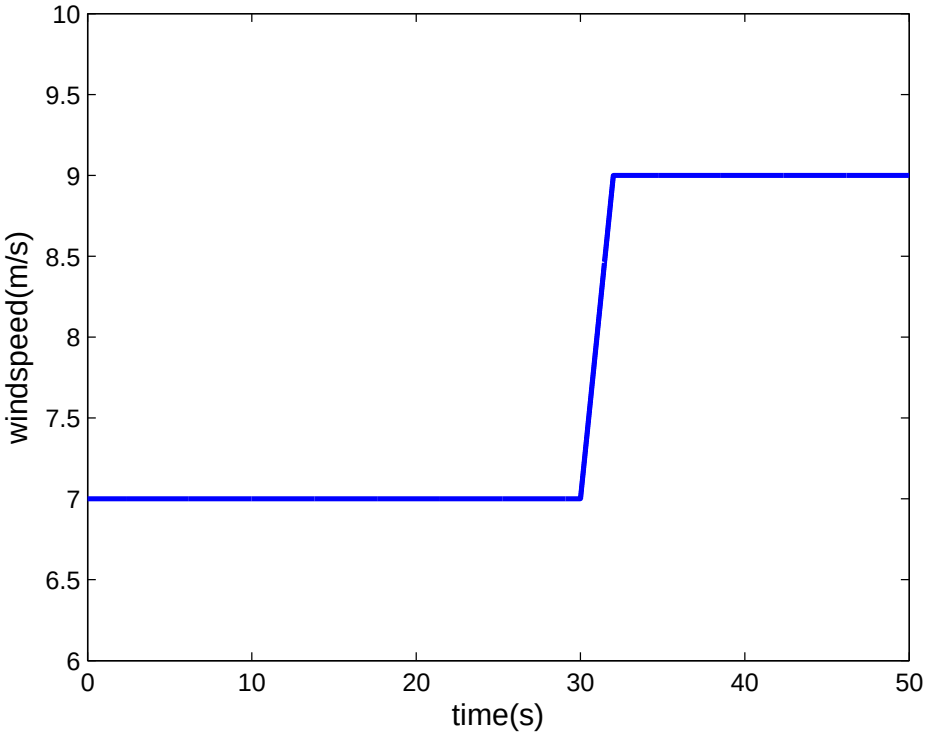

Figure 5.2: Wind Profile

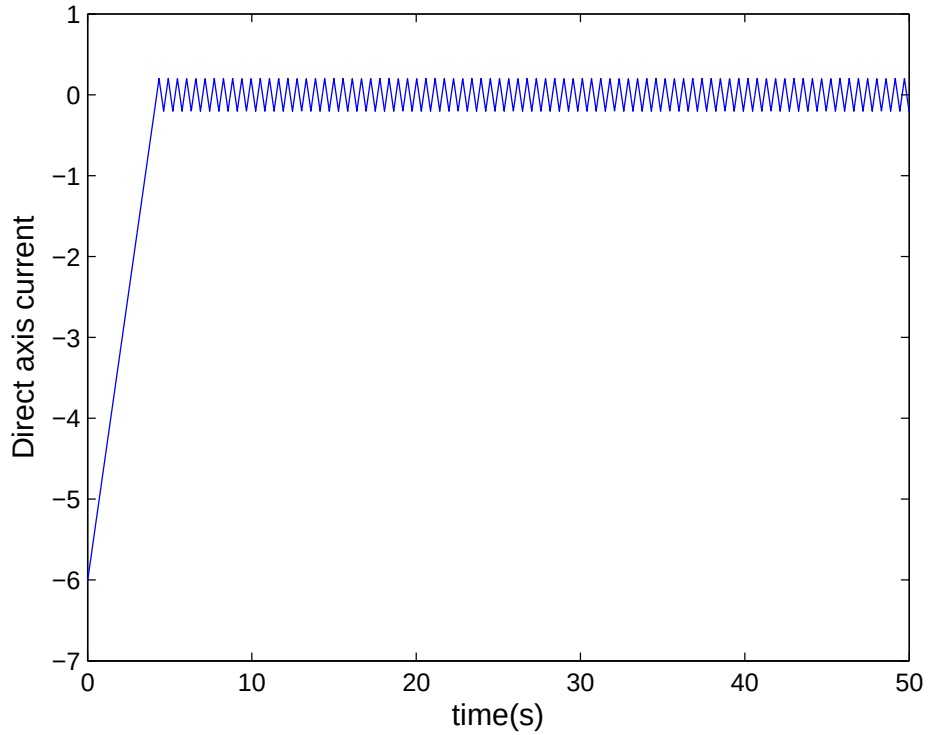

Figure 5.3: *d*-axis Current

The desired value for the direct-axis current is zero amperes (A). Fig. 5.3 demonstrates that the proposed d-axis controller results in the state trajectory of the d-axis current remaining bound to the manifold at $0A$. Even given the drastic change in the wind input, the d-axis controller sufficiently rejects the affect of the disturbance, and maintains the desired state throughout the simulations time.

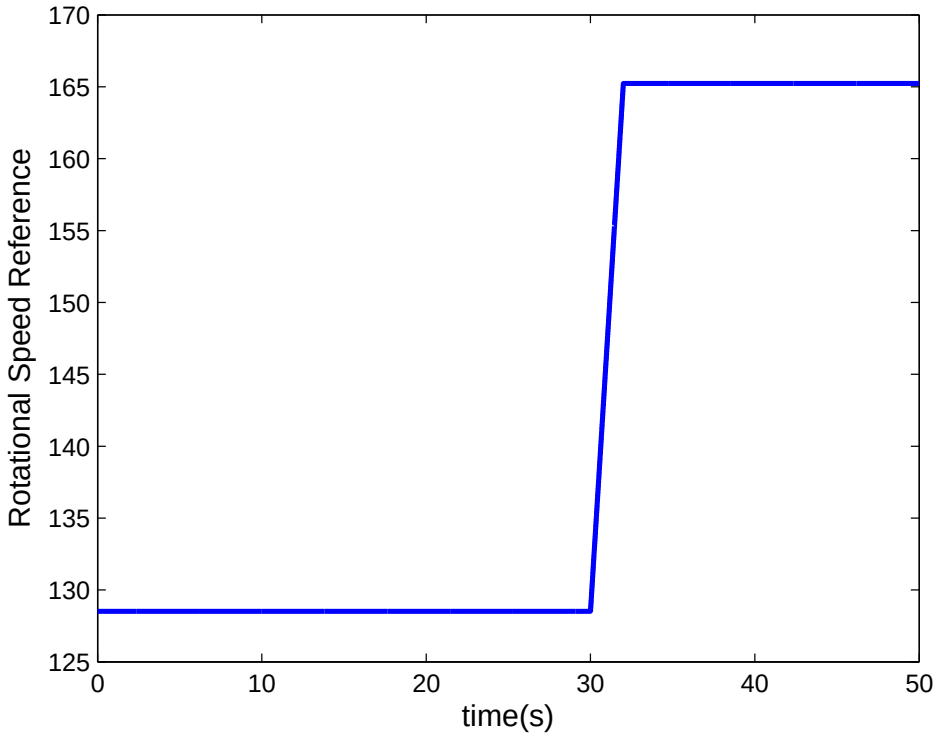

Figure 5.4: Rotational Speed Reference

Figures 5.4 and 5.5 show the shaft rotational speed reference and state behavior throughout the simulation. The effect of the equivalent control can be seen in the rotational speed rise up to the steady state value associated with the initial wind speed. Upon reaching the sliding surface, the tracking ability of the controller is demonstrated during the disturbance. Response time can be increased, but with increased chattering. So, the gains of the controllers were tuned to minimized this effect.

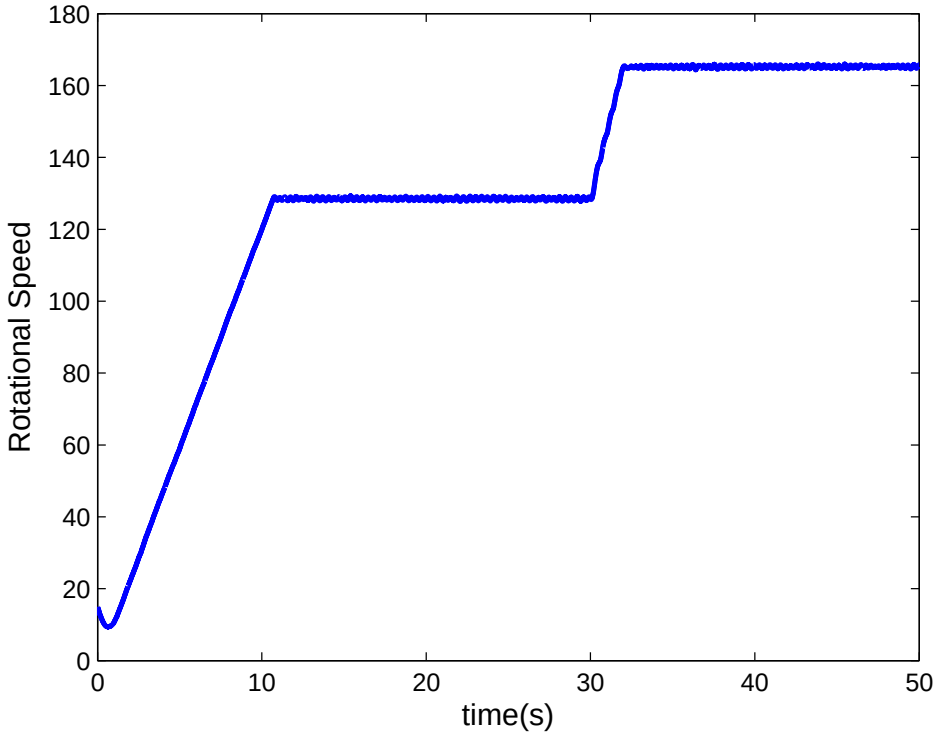

Figure 5.5: Rotational Speed

The quadrature axis current should have a trajectory that follows the same profile as the wind input. This is due to the fact that the reference value of the q-axis current, shown by Fig. 5.6 is dependent on the rotational speed of shaft. Fig. 5.7 shows that the q-axis controller ensures the state of the q-axis current, upon reaching the sliding surface accurately tracks the changing reference. As in the d-axis controller, the chattering effect is more noticeable here. The controller gains were tuned in order to achieve an acceptable compromise between chattering magnitude and response time.

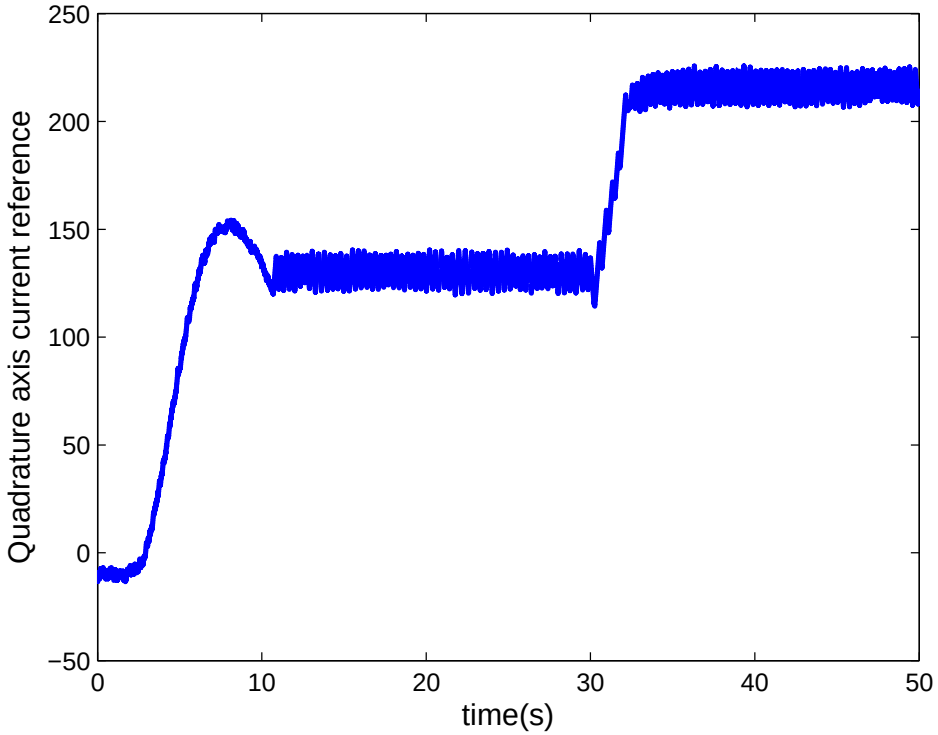

Figure 5.6: q-axis Current Reference

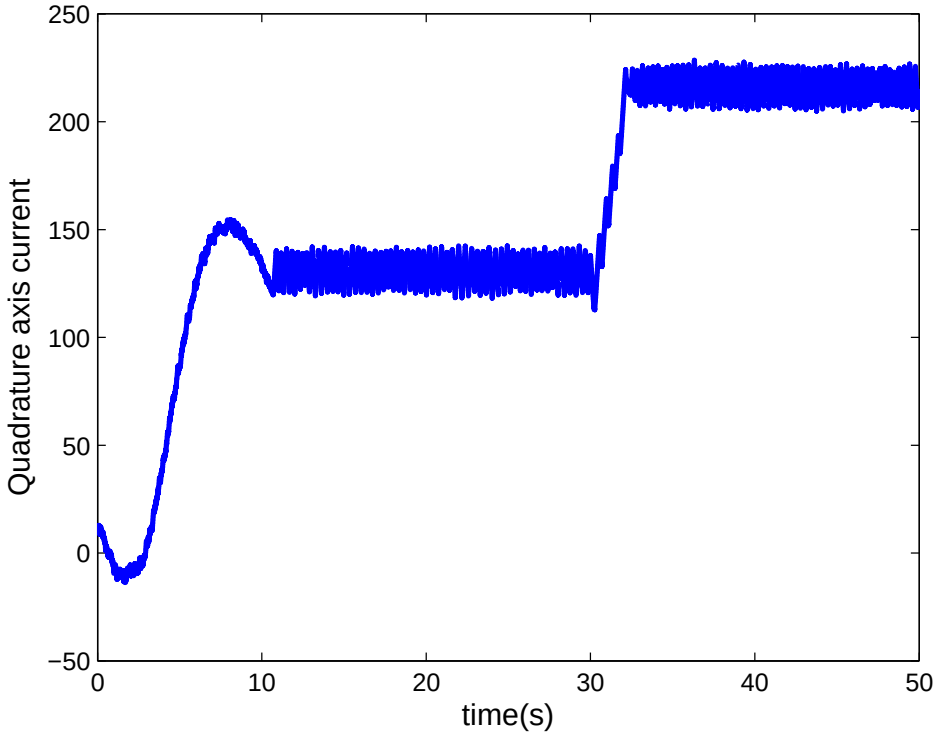

Figure 5.7: q-axis Current

Lastly, Fig. 5.8 represents the efficiency of MPPT for this simulation.

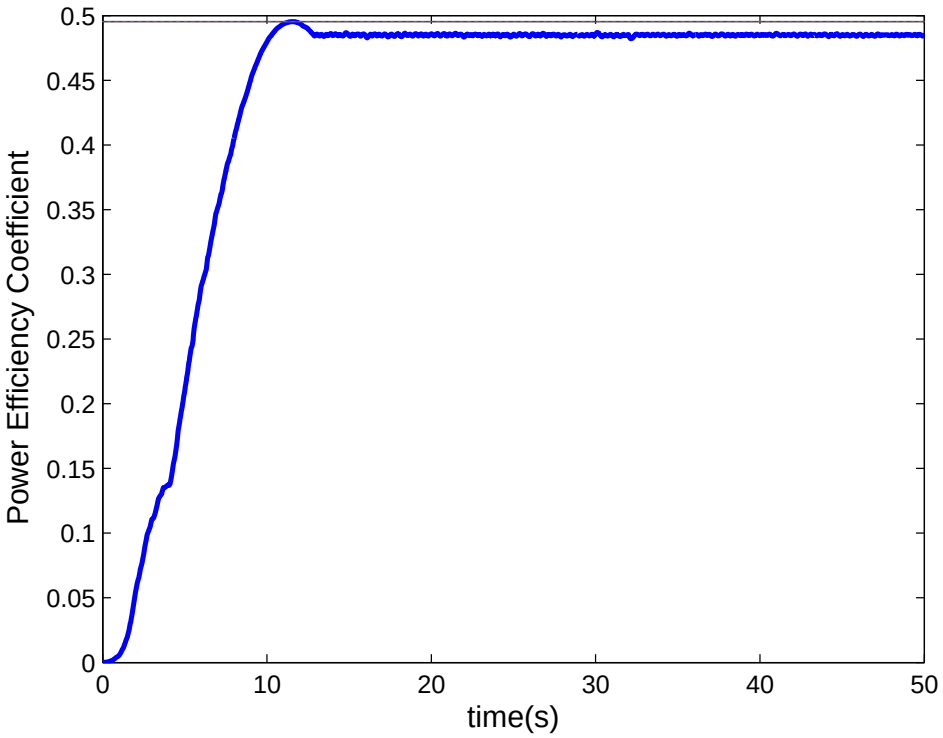

Figure 5.8: $C_p(\lambda)$ v.s. Time

5.8.2 Simulation 2: maximum power point tracking

Simulation 2 demonstrates the tracking ability of the designed control system. A highly varying wind input is presented to the system. The wind profile used is given by Fig. 5.9

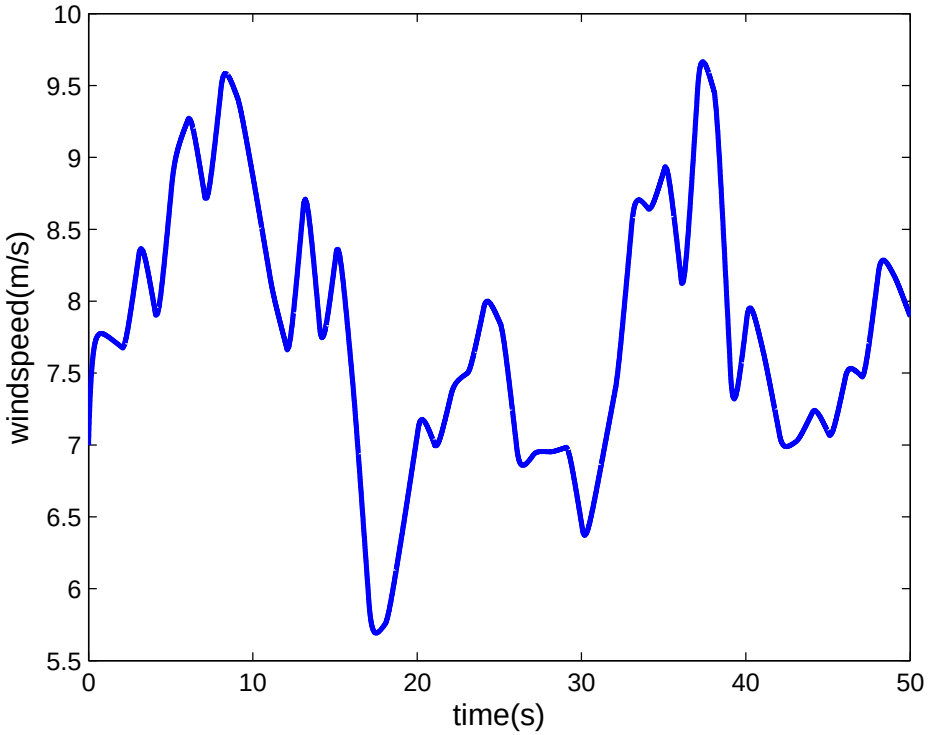

Figure 5.9: Wind Profile 2

As previously stated, the reference value $i_d * (t) = 0$. Fig. 5.10 shows that upon reaching the manifold, the state remains within a bounded area around it throughout the simulation.

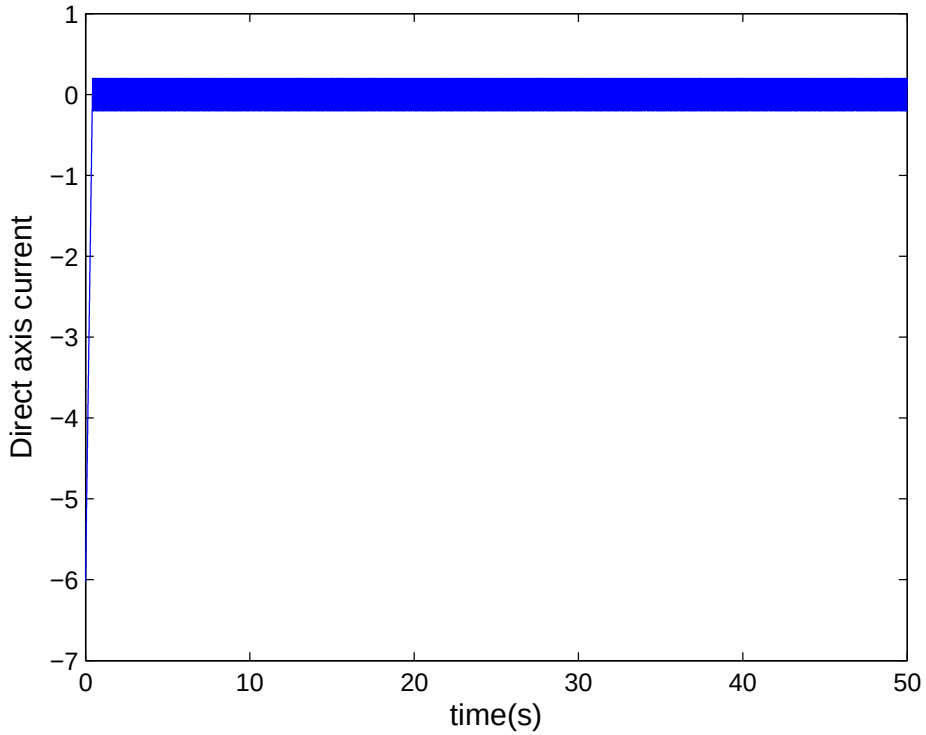

Figure 5.10: d-axis Current

The following Figures 5.11 and 5.12 show the q-axis current reference and state values over the course of the simulation. Due to the dependence of the reference value on the rotational speed control, it is expected that the reference for the q-axis current must change, in order to achieve a constant MPPT.

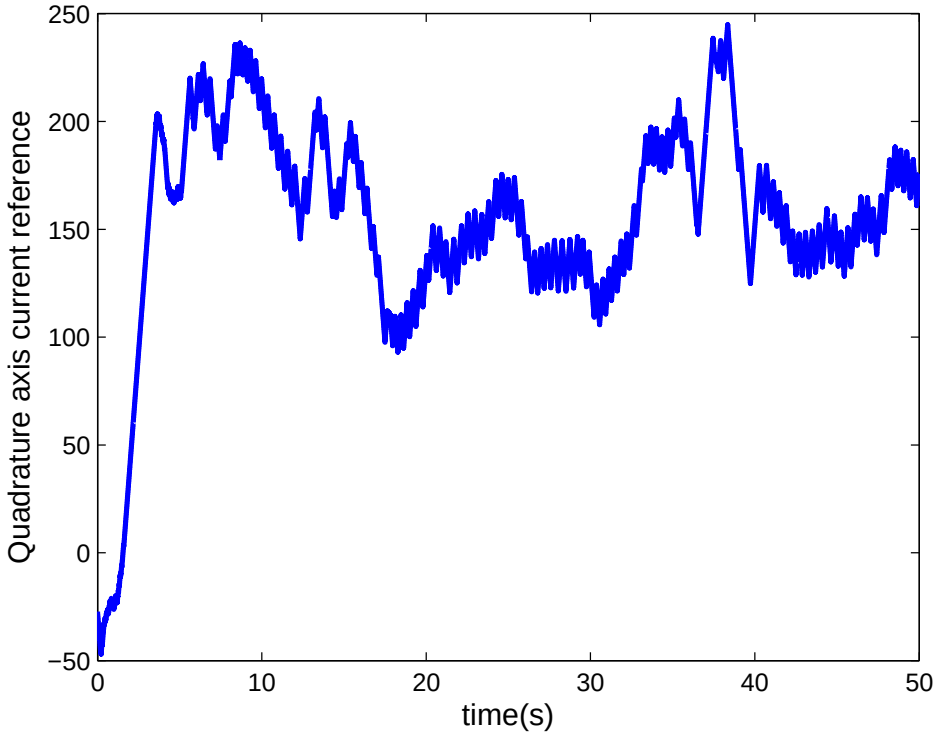

Figure 5.11: q-axis Current Reference

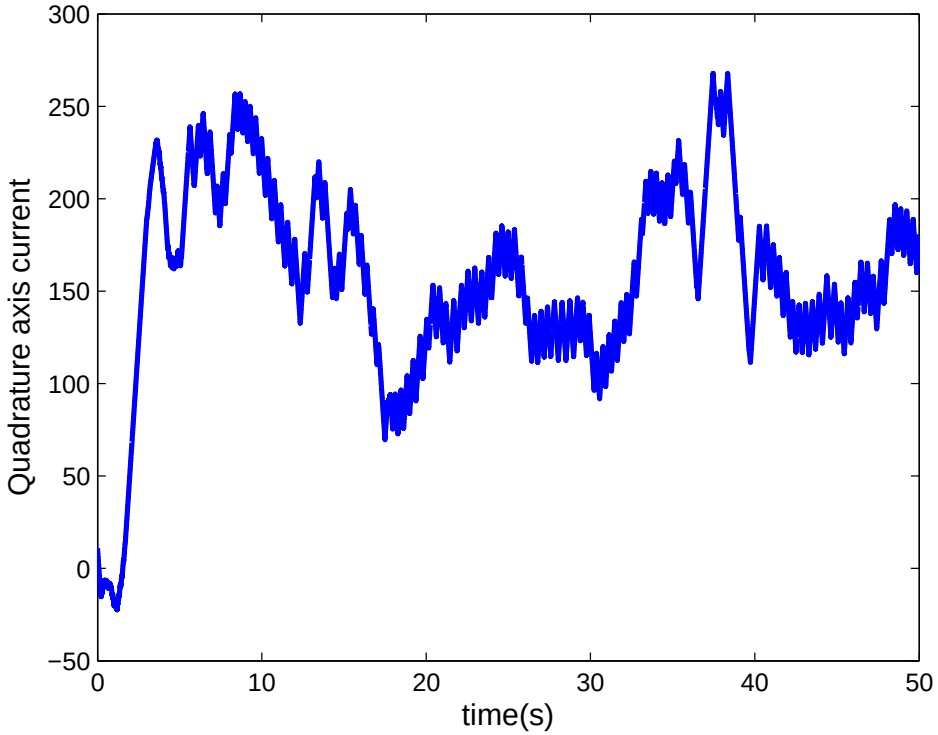

Figure 5.12: q-axis Current

The sliding mode behavior is different for the q-axis current and rotational speed. The reference values for these states change constantly due to the changing wind speed.

Lastly, Fig. 5.14 demonstrates the tracking of the state of the rotational speed given its reference Fig. 5.13

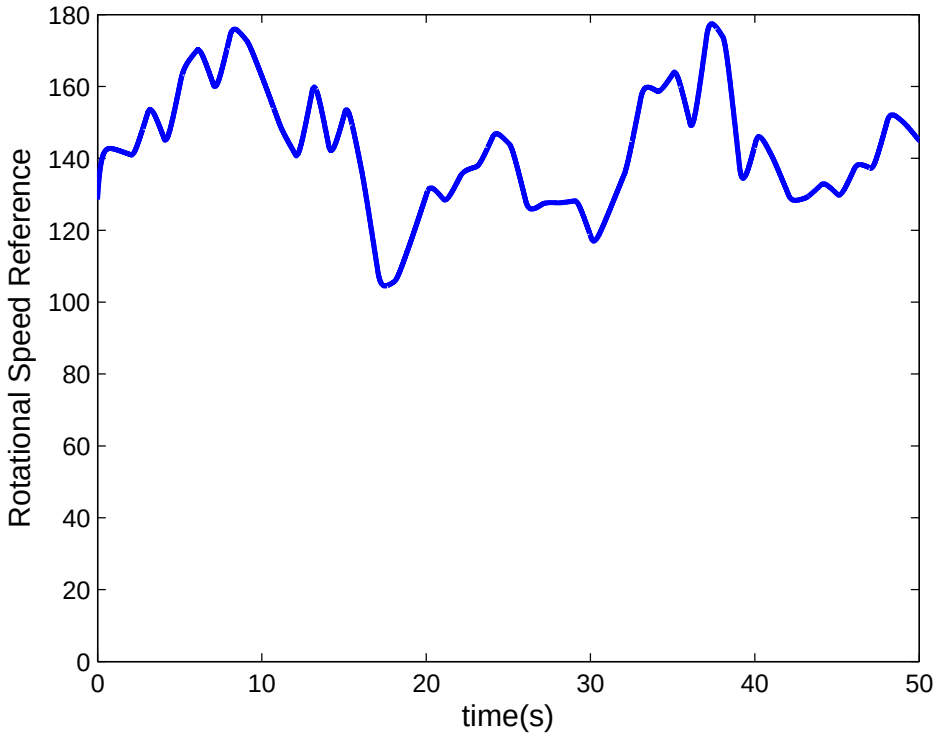

Figure 5.13: Rotational Speed Reference

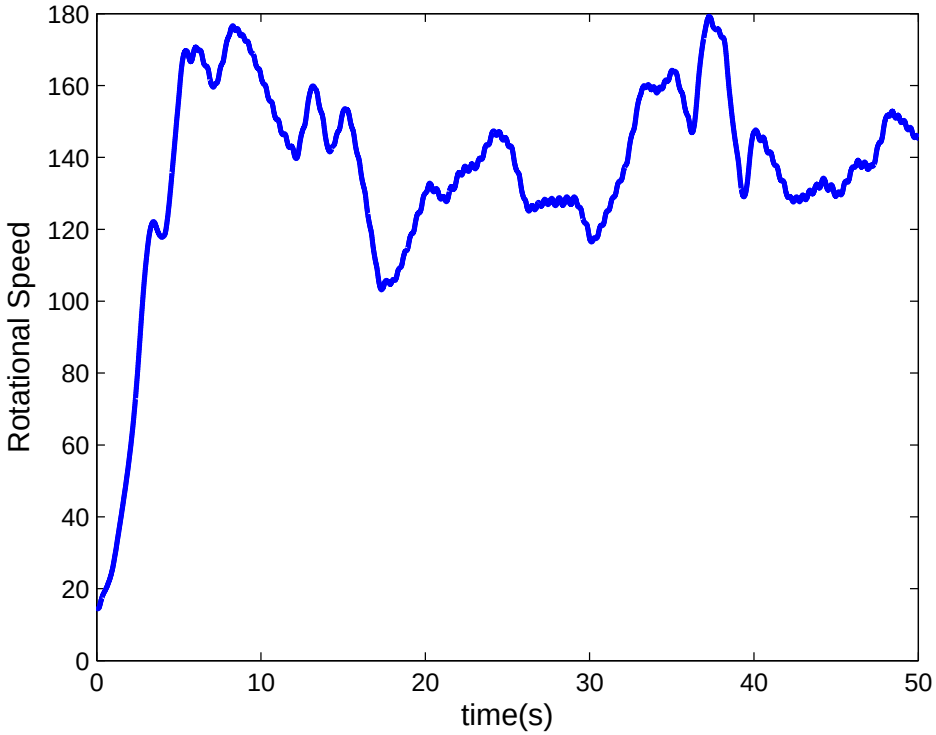

Figure 5.14: Rotational Speed

The ultimate result to be taken from this simulation is the $C_p(\lambda)$ v.s. time curve given by Fig. 5.15. This shows that that given the highly varying wind input used for this simulation, the controller is able to be tuned to achieve a relatively constant MPPT efficiency just above 48%, which shows little deviation over the course of the simulation.

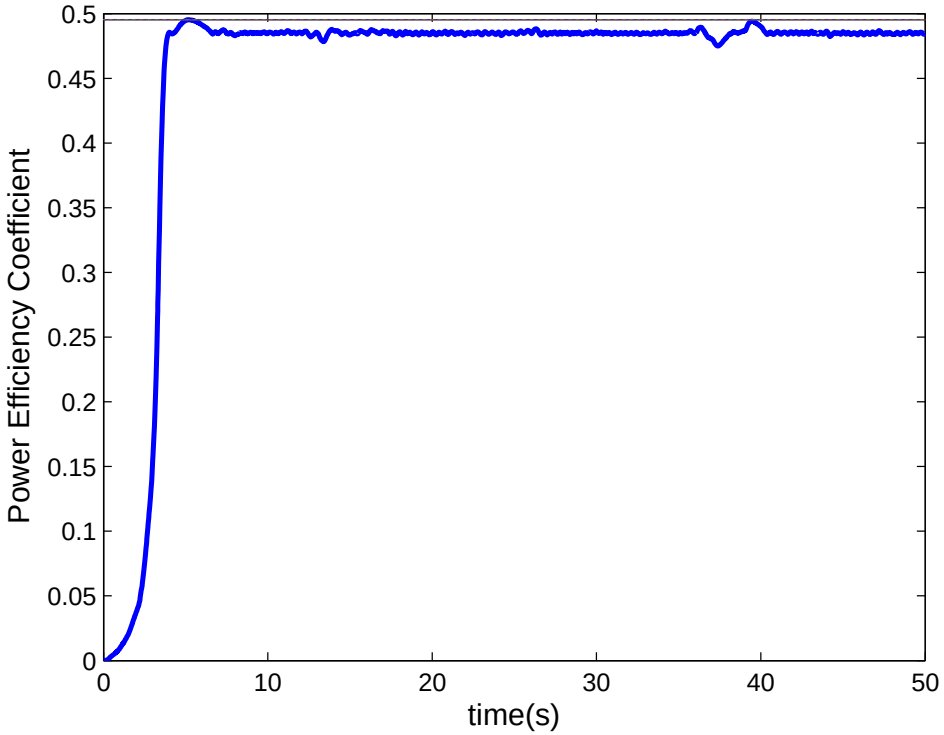

Figure 5.15: $C_p(\lambda)$ v.s. Time

CHAPTER 6

CONTINUOUS TIME FINITE-TIME BOUNDEDNESS AND ROBUST CONTROL USING LINEAR MATRIX INEQUALITIES

The control design in his work combines the aforementioned performance goals of FTB and H_∞ to develop a new LMI control technique for continuous-time and discrete-time systems. The design seeks to ensure robustness and boundedness in the presence of undesired system dynamics. Subsequent application of the method in field oriented control (FOC) of a permanent magnet synchronous generator (PMSG) seeks to solidify the applicability of the new controller.

6.1 Controller Design

The LMI for the stated performance criteria is developed as follows: Given positive matrices $P_1 > 0$ and $P_2 > 0$, consider a quadratic Lyapunov function candidate, and its corresponding derivative given by

$$V(x, w) = x^T P_1 x + w^T P_2 w \tag{6.1}$$

$$\dot{V}(x, w) = 2\dot{x}^T P_1 x + 2\dot{w}^T P_2 w. \tag{6.2}$$

In order to ensure the FTB and H_∞ performance objectives, the following inequality must hold true:

$$\dot{V}(x, w) - \alpha V(x, w) + z^T z - \gamma^2 w^T w < 0 \tag{6.3}$$

From the system given by (4.1a), (4.1b), and (4.2), and from the linear state feedback control given by (4.6) inequality (6.3) becomes

$$\begin{aligned} x^T[&2(A^T + \Delta A^T + K^T B^T + K^T \Delta B^T - \alpha)P_1 \\ &+ (C^T + K^T D^T)(C + DK)]x + 2w^T \Phi^T P_2 \Phi x \\ &+ w^T[(2\Phi^T - \alpha)P_2 - \gamma^2]w < 0 \end{aligned} \tag{6.4}$$

Noting that $2M^TN = NM + M^TN$ for appropiatly sized matricies M and N, inequality can be re-written as

$$\begin{bmatrix} x^T & w^T \end{bmatrix} \begin{bmatrix} P_1A + A^TP_1 + P_1\Delta A + \Delta A^TP_1 & \\ +P_1B + B^TP_1 + P_1\Delta B + \Delta B^TP_1 & F + \Delta F \\ +(C^T + K^TD^T)(C + DK) & \\ & \\ F^T + \Delta F^T & P_2\Phi + \Phi^TP_2 \\ & -\alpha P_2 - \gamma^2 I \end{bmatrix} \begin{bmatrix} x \\ w \end{bmatrix} < 0. \tag{6.5}$$

From (6.5), the following matrix inequality can be obtained as

$$\begin{bmatrix} P_1A + A^TP_1 + P_1\Delta A + \Delta A^TP_1 & \\ +P_1B + B^TP_1 + P_1\Delta B + \Delta B^TP_1 & F + \Delta F \\ -\alpha P_1 + (C^T + K^TD^T)(C + DK) & \\ & \\ F^T + \Delta F^T & P_2\Phi + \Phi^TP_2 - \alpha P_2 - \gamma^2 I \end{bmatrix} < 0. \tag{6.6}$$

It is now desired to employ the assumptions made about bounded disturbances by (4.3), (4.4), and (4.5). The first step is to pre- and post-multiply the inequality by

$$\begin{bmatrix} P_1^{-1} & 0 \\ 0 & I \end{bmatrix}. \tag{6.7}$$

For simplicity sake, let $X = P_1^{-1}$, and $Y = KP_1^{-1}$. It follows that (6.6) becomes

$$\begin{bmatrix} AX + XA^T + BY + Y^TB^T & \\ +\Delta AX + X\Delta A^T + \Delta BY + Y^T\Delta B^T & F + \Delta F \\ -\alpha X + (C^T + K^TD^t)(C + DK) & \\ & \\ F^T + \Delta F & P_2\Phi + \Phi^TP_2 - \alpha P_2 - \gamma^2 I \end{bmatrix} < 0. \tag{6.8}$$

From Lemma 4.7, the following two inequalities can be formulated:

$$\begin{aligned}
&\begin{bmatrix} 0 & \Delta F \\ \Delta F^T & 0 \end{bmatrix} \\
&\leq \begin{bmatrix} \alpha_1 \Delta F \Delta F^T & 0 \\ 0 & \alpha_1^{-1} I \end{bmatrix} \\
&\leq \begin{bmatrix} \alpha_1 \sigma_F^2 I & 0 \\ 0 & \alpha_1^{-1} I \end{bmatrix}
\end{aligned} \tag{6.9}$$

$$\begin{aligned}
&\begin{bmatrix} \Delta A X + X \Delta A^T & 0 \\ +\Delta B Y + Y^T \Delta B^T & \\ 0 & 0 \end{bmatrix} \\
&\leq \begin{bmatrix} \alpha_2^{-1} X X + \alpha_2 \Delta A \Delta A^T & 0 \\ +\alpha_3 \Delta B \Delta B^T + \alpha_3^{-1} Y Y^T & \\ 0 & 0 \end{bmatrix} \\
&\leq \begin{bmatrix} \alpha_2 \sigma_A^2 I + \alpha_2^{-1} X X & 0 \\ +\alpha_3 \sigma_B^2 I + \alpha_3^{-1} Y^T Y & \\ 0 & 0 \end{bmatrix}
\end{aligned} \tag{6.10}$$

Based on the conditions developed by (6.9) and (6.10), (6.8) is re-given as follows:

$$\begin{bmatrix} AX + XA^T + BY + Y^T B^T + \alpha_2^{-1} XX & & \\ +\alpha_3^{-1} Y^T Y + \alpha_1 \sigma_F^2 I + \alpha_2 \sigma_A^2 I + \alpha_3 \sigma_B^2 I & & F \\ -\alpha X + (XC^T + Y^T D^T)(CX + DY) & & \\ & & \\ F^T & & P_2 \Phi + \Phi^T P_2 - \alpha P_2 \\ & & -\gamma^2 I + \alpha_1^{-1} I \end{bmatrix} < 0. \tag{6.11}$$

At this point the inequality still contains non-linear terms. The application of Schur Complement allows for the linearizion of the matrix inequality. Through this, the matrix inequality (6.11) can be transformed into the linear matrix inequality, and subsequently the final result of the derivation. Therefore, if the solution of following inequality given by

$$\begin{bmatrix} AX + XA^T & & & & \\ +BY + Y^TB^T - \alpha X & F & XC^T + Y^TD^T & X & Y \\ +\alpha_1\sigma_F^2 I + \alpha_2\sigma_A^2 I + \alpha_3\sigma_B^2 I & & & & \\ F^T & P_2\Phi + \Phi^T P_2 & 0 & 0 & 0 \\ & -\alpha P_2 - \gamma^2 I + \alpha_1^{-1} I & & & \\ CX + DY & 0 & -I & 0 & 0 \\ X & 0 & 0 & -\alpha_2 I & 0 \\ Y^T & 0 & 0 & 0 & -\alpha_3 I \end{bmatrix} < 0 \tag{6.12}$$

is found to exist, then the system is FTB in the presence of bounded disturbances. Also, the H_∞ performance specifications are satisfied, which results in robustness given model parameter uncertainties and disturbances.

6.2 Simulation Results

The following simulations use the (d, q) coordinate frame model of the PMSG developed in Chapter 2; given by (2.26) and (2.27). The LMI Editor GUI, which is part of the Robust Control Toolbox in MATLAB was utilized to implement the LMI. The system was implemented, with initial state disutrbances for i_d and i_q. The consant parameters of the LMI were adjusted in order to obtain a feasible solution that guarantees the design

goals of the control method, and provides a sufficiently fast disurbance response. The simulation results are shown in Fig. 6.1 through Fig. 6.3.

For initial disurbances imposed upon the state, the state trajectories are asymptotically stable, and driven towards the reference value in a timerly manner. The images demonstrate the satisfaction FTB and H_∞ performance criteria. For a single speed in the WECs application.

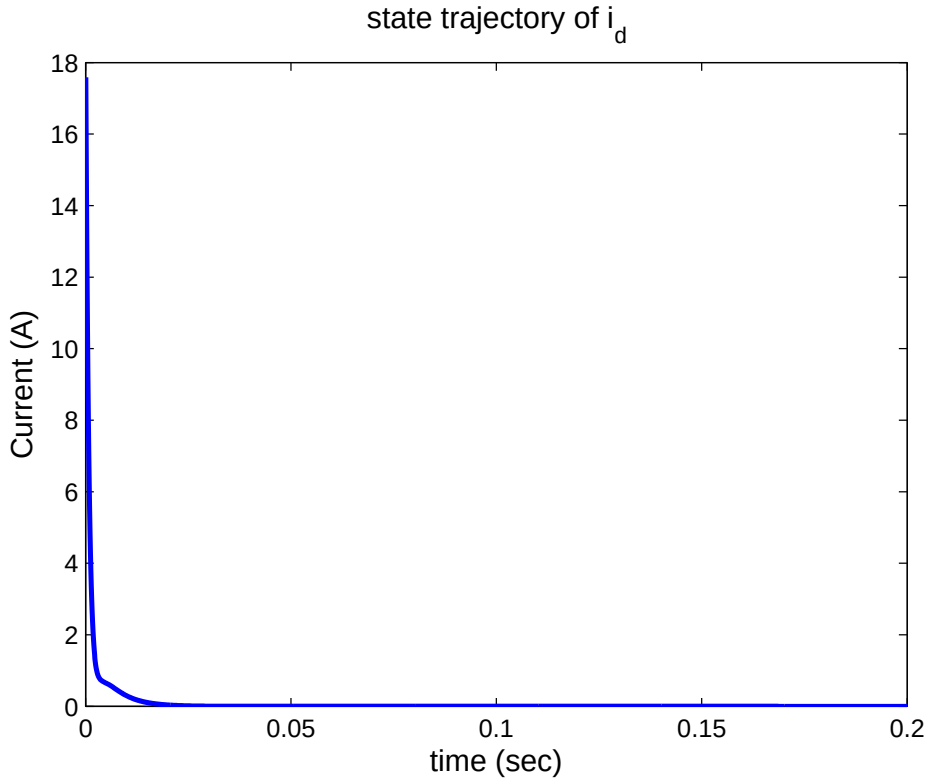

Figure 6.1: *d*-axis Current

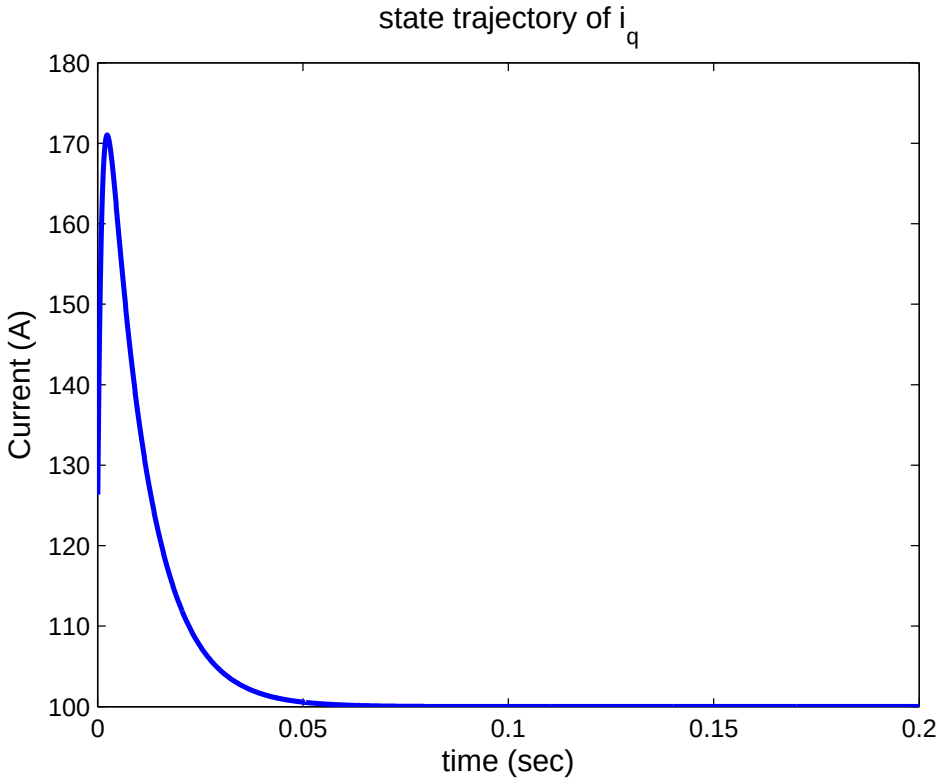

Figure 6.2: q-axis Current

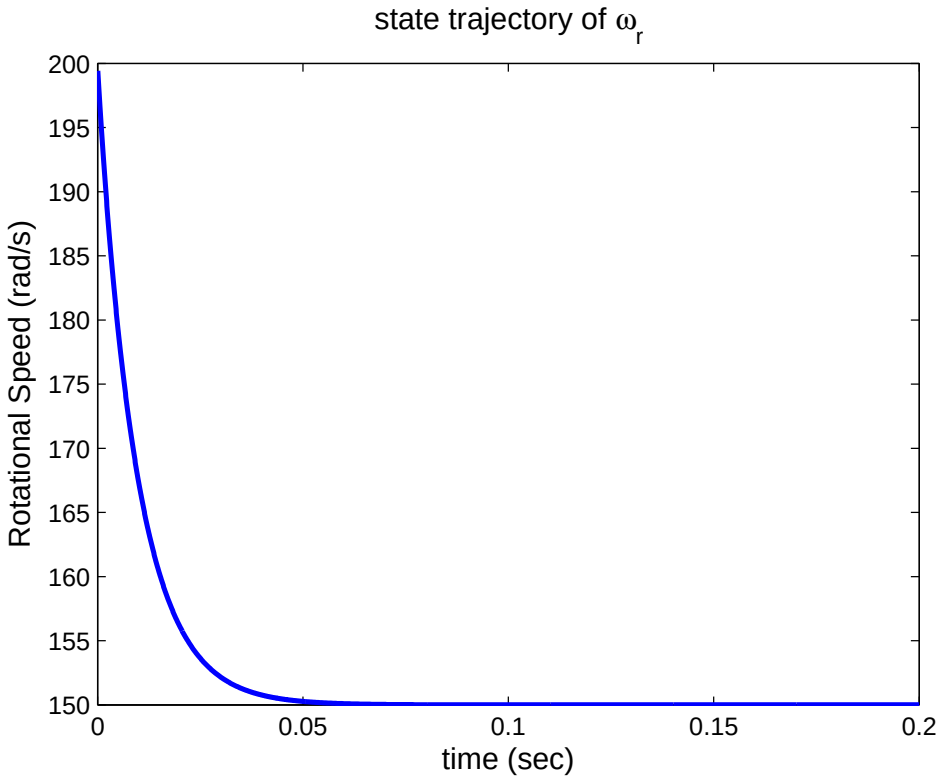

Figure 6.3: Rotational Speed

CHAPTER 7

DISCRETE-TIME FINITE-TIME BOUNDEDNESS USING LINEAR MATRIX INEQUALITIES

Using the discrete-time system given in chapter 4, the following gives the existing work on the discrete-time LMI guaranteeing the FTB and H_∞ performance objectives.

Given positive matrices $P_1 > 0$ and $P_2 > 0$, consider the following discrete-time quadratic Lyapunov candidate, and it's discrete-time derivative

$$v_k = x_k^T P_1 x_k + w_k^T P_2 w_k \tag{7.1}$$

$$v_{k+1} = x_{k+1}^T P_1 x_{k+1} + w_{k+1}^T P_2 w_{k+1} \tag{7.2}$$

In order to satisfy FTB, the following inequality must be satisfied:

$$v_{k+1} < \alpha v_k, \forall\ k \in \mathbb{N}_0, \tag{7.3}$$

where $\alpha \leq 1$. Neglecting bounded uncertainties, the inequality becomes

$$x_{k+1}^T P_1 x_{k+1} + w_{k+1}^T P_2 w_{k+1} < \alpha(x_k^T P_2 x_k + w_k^T P_2 w_k) \tag{7.4}$$

From (4.7a), (4.7b), and (4.7d), (7.4) can be re-written as

$$\begin{aligned} &x_k^T (A^T + K^T B^T) P1 (A + BK) x_k + x_k^T (A^T + K^T B^T) P_1 F w_k \\ &\quad + w_k^T F^T P_1 (A + BK) x_k + w_k^T F^T P_1 F w_k + w_K^T \phi^T P_2 \phi w_k \\ &\quad < \alpha(x_k^T P_1 x_k + w_k^T P_2 w_k) \end{aligned} \tag{7.5}$$

In matrix form, inequality (7.5) becomes

$$\begin{aligned} \begin{bmatrix} x_k & w_k \end{bmatrix}^T &\begin{bmatrix} (A^T + K^T B^T) P_1 (A + BK) & (A^T + K^T B^T) P_1 F \\ F^T P_1 (A + BK) & F^T P_1 F + \phi P_2 \phi \end{bmatrix} \begin{bmatrix} x_k \\ w_k \end{bmatrix} \\ &< \begin{bmatrix} x_k & w_k \end{bmatrix}^T \begin{bmatrix} \alpha P_1 & 0 \\ 0 & \alpha P_2 \end{bmatrix} \begin{bmatrix} x_k \\ w_k \end{bmatrix} \end{aligned} \tag{7.6}$$

Extracting the variables, and re-orienting the terms to one side, the matrix inequality can be given equivalently as

$$\begin{bmatrix} \alpha P_1 - A^T P_1 A - A^T P_1 BK & -(A^T P_1 F + K^T B^T P_1 F) \\ -K^T B^T P_1 A - K^T B^T P_1 BK & \\ & \\ -(F^T P_1 A + F^T P_1 BK) & \alpha P_2 - F^T P_1 F - \phi P_2 \phi \end{bmatrix} > 0. \tag{7.7}$$

Next, consider the H_∞ performance criterion. It is necessary to re-define H_∞ for discrete-time applications.

Definition 7.1. The following inequality must hold true:

$$V_{k+1} < \alpha V_k, \tag{7.8}$$

for $\alpha \leq 1$. From (4.7c) and (4.7b), inequality (7.8) becomes

$$z_k^T z_k - \gamma^2 w_k^T w_k + V_{k+1} - \alpha V_k < 0, \tag{7.9}$$

Applying Definition (7.1), it follows that

$$(Cx_k + Du_k)^T (Cx_k + Du_k) - \gamma^2 w_k^T w_k + V_{k+1} - \alpha V_k < 0. \tag{7.10}$$

Combining this with the LMI for FTB, (7.7) becomes

$$\begin{bmatrix} -A^T P_1 A - A^T P_1 BK & & \\ -K^T B^T P_1 A - K^T B^T P_1 BK & -A^T P_1 F - K^T B^T P_1 F & \\ -(C + DK)^T (C + DK) + \alpha P_1 & & \\ & & \\ -F^T P_1 A - F^T P_1 BK & \alpha P_2 - F^T P_1 F & \\ & -\phi P_2 \phi - \gamma^2 I & \end{bmatrix} > 0. \tag{7.11}$$

In order to separate the nonlinear terms in the inequality, Schur complement is applied, and (7.11) becomes

$$\begin{bmatrix} \alpha P_1 - C^T D K - K^T D^T C - C^T C - K^T D^T D K & 0 & A^T + K^T B^T \\ 0 & \alpha P_2 + \gamma^2 I - \phi P_2 \phi & F^T \\ A + BK & F & P_1^{-1} \end{bmatrix} > 0 \tag{7.12}$$

Next, pre- and post-multiply inequality (7.12) by

$$\begin{bmatrix} P_1^{-1} & 0 & 0 \\ 0 & I & 0 \\ 0 & 0 & I \end{bmatrix}, \tag{7.13}$$

and let $X = P_1^{-1}$ and $Y = KP_1^{-1}$. It follows that (7.12) becomes

$$\begin{bmatrix} \alpha X - XC^T DY - Y^T D^T CX - XC^T CX - Y^T D^T DY & 0 & XA^T + Y^T B^T \\ AX + BY & F & X \end{bmatrix} > 0. \tag{7.14}$$

Lastly, the applciation of Schur complement to (7.14) provides the following LMI result

$$\begin{bmatrix} \alpha X & 0 & XA^T + Y^T B & XC^T + Y^T D \\ 0 & \alpha P_2 + \gamma^2 I - \phi P_2 \phi & F^T & 0 \\ AX + BY & F & X & 0 \\ CX + DY & 0 & 0 & I \end{bmatrix} > 0, \tag{7.15}$$

which is FTB and robust given external disturbances.

CHAPTER 8

CONCLUSION AND FUTURE WORK

8.1 Conclusion

Global interest in moving away from the use of fossil fuels as the primary source for electric power generation has lead to a vested interest in wind energy technology. Increased use of, and interest in variable-speed wind energy conversion systems have created due cause for research in the global control systems engineering community.

This work first presented the application of various control systems techniques in a model application of a VS-WECS using a permanent magnet synchronous generator. Sliding mode control is given in the context of field oriented and speed control of the model. The results of extensive simulations show that this method can be implemented in order to achieve a higher level of maximum power point tracking and disturbance rejection. Moreover, experimentation using wind profiles of varying intensity show that this control scheme is applicable over a significant range of input conditions. Only minor gain adjustments are necessary in order to maximize response while minimizing the magnitude of switching delay effects. The results of this controller have been published in [50]

Furthermore, the combination of H_∞ and finite-time boundedness performance criteria, achieved through the use of LMIs, are applied to the VS-WECS model. Simulations in stability analysis and disturbance rejection help to exhibit the effectiveness of the proposed design. LMIs, already proven to be a powerful method for complex system control, provide a seemingly effective medium for the implementation of the desired performance objectives.

8.2 Future Work

The results presented here seek to demonstrate the potential of the proposed control methods. However, they do not fully encompass the entire scope challenges associated VS-WECS and PMSG control. Future work into the proposed sliding mode control architecture should include analysis of conditions such as loading, grid connections, and faults; eventually leading to actual implementation of the proposed control schemes. Where, expansion upon the performance of the Continuous-TIME LMI based control scheme should demonstrate the effectiveness of this control scheme over dynamic wind profiles. Further development is neccessary for the discrete-time LMI to include bounded parametric uncertainties. Simulations involving of the discrete-time LMI would also provide foundational evidence in support of this methodology. It is hoped that the results presented in this work will serve to incrementally build upon the prior research in VS-WECS, PMSG control, and even dynamical systems control fields.

REFERENCES

[1] R.E.H. Sims. Renewable energy: a response to climate change. *Solar World Congress*, 76:9–17, Mar. 2004.

[2] D. Greene. Measuring energy security: can the united states achieve oil independence? *Energy Security*, 38:1614–1621, April 2010.

[3] J. Hughes. Energy; a reality check on the shale revolution. *Nature*, 494:307–308, February 2013.

[4] F. Sissine. *Energy independence and security act of 2007: a summary of major provisions*. USA, December 2007.

[5] I. Munteanu. *Optimal Control of Wind Energy Systems*. Springer, London, 2008.

[6] Y. Errami and et al. Maximum power point tracking strategy and direct torque control of permanent magnet synchronous generator wind farm. *International Conference on Complex Systems*, pages 1–6, November 2012.

[7] Scott Semken and et al. Direct-drive permanent magnet generators for high-power wind turbines: benefits and liiting factors. June 2011.

[8] A. Farhan, A. Saleh, and A. Shaltout. Higher performance reluctance synchronous motor drive using field oriented control. *International Conference on Modelling, Identification, and Control*, pages 181–186, September 2013.

[9] M. Garcia-Sanz and M. Maaroufi. *Wind Energy Systems Control Engineering Design*. Taylor and Francis Group, LLC., Boca Raton, 2012.

[10] M. Ragheb and A. M. Ragheb. *Wind Turbines Theory - The Betz equation and Optimal Rotor Tip Speed Ratio, Fundamental and Advanced Topics in Wind Power*. Dr. Rupp Carriveau (Ed.), http://www.intechopen.com/books/fundamental-and-advanced-topics-in-wind-power/wind-turbines-theory-the-betz-equation-and-optimal-rotor-tip-speed-ratio, 2011.

[11] Ieee guide for synchronous generator modeling practices and applications in power system stability analyses. *IEEE Std 1110-2002 (Revision of IEEE Std 1110-1991)*, pages 1–72, 2003.

[12] M.J. Basler, A. Gohwhani, P. Rao, and J. Burnworth. *Excitation Control Systems Second Edition*. Lightning Press, Totowa, New Jersey, 2001.

[13] H. Haraguchi, S. Morimoto, and M. Sanada. Suitable design of a pmsg for large-scale wind power generator. pages 2447–2452, September 2009.

[14] V. Utkin, J. Guldner, and J. Shi. *Sliding Mode Control in Electromechanical Systems*. Taylor & Francis, Philidelphia, Pennsylvania, 1999.

[15] M. Zhihong and X.H. Yu. Terminal sliding mode control of mimo linear systems. November 1997.

[16] X. Zhang, L. Sun, and K. Zhao. Nonlinear speed control for pmsm system using sliding-mode control and disturbance compensation techniques. March 2013.

[17] H.K. Khalil. *Nonlinear Systems Third Edition*. Prentice Hall, Upper Saddle River, NJ, 2002.

[18] S.C. Tan, Y.M. Lai, and C.K. Tse. *Sliding Mode Control of Switching Power Converters*. CRC Press, Taylor & Francis Group, 2012.

[19] A.J. Koshkouei, K.J. Burnham, and A.S.I. Zinober. Dynamic sliding mode control design. July 2015.

[20] L. Shihua, M. Zhou, and X. Yu. Design and implementation of terminal sliding mode control method for pmsm speed regulation system. 28, NO. 3:1358–1365, November 2014.

[21] B. Beltran, T. Ahmed-Ali, and M.E.H. Benbouzid. High-order sliding-mode control variable-speed windturbines. 56, NO. 9:3314–3321, September 2009.

[22] B. Beltran, T. Ahmed-Ali, and M.E.H. Benbouzid. Sliding mode power control of variable-speed wind energy conversion systems. June 2008.

[23] Y. Feng and et al. Terminal sliding mode control of induction generator for wind energy conversion systems. pages 4741–4746.

[24] M.I. Martinez, A. Susperregui, and Xu L. Tapia, G. Sliding-mode control of a wind turbine-driven double-fed induction generator under non-ideal grid voltages. pages 370–379.

[25] O.A. Morfin, A.G. Loukianov, and J.M. Cañedo. Robust non-linear control of wound rotor induction generator: Integral sliding modes. pages 1–6, September 2008.

[26] Y. Errami and et al. Nonlinear control of mppt and grid connected for wind power generation systems based on the pmsg. May 2013.

[27] C. Scherer and W. Siep. Linear matrix inequalities in control. pages 1–27. Delft University of Technology and Eindhoven University of Technology, 2004.

[28] S. Boyed, L.E. Ghaoui, E. Feron, and V. Balakrishnan. Linear matrix inequalities in system and control theory. pages 1–7. Society for Industrial and Applied Mathematics, Philadelphia, 1994.

[29] X. Yu and K. Tomsovic. Application of linear matrix inequalities for load frequency control with communication delays. *IEEE Transactions on Power Systems*, pages 1508–1515, 2004.

[30] A.F. Snyder and et al. A robust damping controller for power systems using linear matrix inequalities. *Power Engineering Society 1999 Winter Meeting, IEEE*, pages 519–524, 1999.

[31] F. Amato, M. Airola, and C. Cosentino. Finite-time stability of linear time-varying systems: Analysis and controller design. *IEEE Transactions on Automatic Control*, pages 1003–1008, 2010.

[32] F. Amato, M. Airola, and P. Dorato. Finite-time control of discrete-time linear systems. *IEEE Transactions on Automatic Control*, 50:724–729, 2005.

[33] F. Amato, C. Cosentino, and A. Merola. Sufficient conditions for finite-time stability and stabilization of nonlinear quadratic systems. *IEEE Transactions on Automatic Control*, 55:430–434, 2010.

[34] F. Amato, M. Airola, and C. Cosentino. Finite-time stabilization via dynamic output feedback. *Automatica*, 42:337–342, 2005.

[35] F. Amato, M. Airola, and P. Dorato. Finite-time control of linear systems subject to parametric uncertainties and disturbances. *Automatica*, 37:1459–1463, 2001.

[36] P Dorato, L. Fortuna, and G. Muscato. *Robust Control for Unstructured Perturbations - An Introduction*. Springer-Verlag, New York, 1992.

[37] Xin Wang, E. E. Yaz, and Y. I. Yaz. Robust and resilient state dependent control of continuous-time nonlinear systems with general performance criteria. *IEEE Conference on Decision and Control*, 37:603–608, 2010.

[38] F. Amato, M. Airola, and P. Dorato. Finite-time control of linear systems subject to parametric uncertainties and disturbances. *Automatica*, 37:1459–1463, 2001.

[39] R. Xie, X. Wang, and Y. Li. H_∞ state feedback control for the stabilization of the three euler angles of helicopter based on lmi. *International Conference on Intelligent Computation Technology and Automation*, pages 375–379, 2008.

[40] P. Dorato. *Short-Time Stability in Linear Time-Varying Systems*. Polytechnic Institute of Brooklyn, New York, 1961.

[41] ElBsat M.N. and Yaz E.E. Robust and resilient finite-time control of a class of discrete-time nonlinear systems. pages 6454–6459, August-September 2011.

[42] M.S. Mahmoud and Y. Xia. *Applied Control Systems Design*. Springer, New York, 2012.

[43] K. Zhou and J. Doyle. *Robust and Optimal Control*. Prentice Hall, Upper Saddle River, New Jersey, 1996.

[44] X. Wang, E.E. Yaz, and J. Long. Robust and resilient state-dependent control of discrete-time nonlinear systems with general performance criteria. *System Science & Control Engineering*, 2:48–54, 2014.

[45] S. Boyd and L. Vandenberghe. *Convex Optimization*. Cambridge University Press, New York, 2009.

[46] Y. Peng, Q.M. Zhu, and H. Nouri. Lmi based h_2/h_∞ power system stabilizers for large disturbances in power systems with wind plant. *International Conference on Modelling, Identification and Control*, pages 939–944, 2012.

[47] C. Sloth, T. Esbensen, Niss M.O.K., J. Stoustrup, and P.F. Odgaard. Robust lmi-based control of wind turbines with parametric uncertainties. *IEEE International Conference on Control Application*, pages 776–781, July 2009.

[48] S. Bououden, M. Chadli, and H.R. Karimi. Robust predictive control of a variable speed wind turbine using the lmi formalism. *European control Conference*, pages 820–825, June 2014.

[49] A.H. Besheer, H.M. Emara, and M.M.A. Aziz. Fuzzy based output feedback control for wind energy conversion system: An lmi approach. *Power Systems Conference and Exposition*, pages 2030–2037, October 2006.

[50] J. Hostettler and X Wang. Sliding mode control of a permanent magnet synchronous generator for variable speed wind energy conversion systems.